

# In-Depth Proteomic Analysis of Paraffin-Embedded Tissue Samples from Colorectal Cancer Patients Revealed TXNDC17 and SLC8A1 as Key Proteins Associated with the Disease

Ana Montero-Calle,\* María Garranzo-Asensio, Carmen Poves, Rodrigo Sanz, Jana Dziakova, Alberto Peláez-García, Vivian de los Ríos, Javier Martínez-Useros, María Jesús Fernández-Aceñero, and Rodrigo Barberas\*



Cite This: *J. Proteome Res.* 2024, 23, 4802–4820



Read Online

ACCESS |

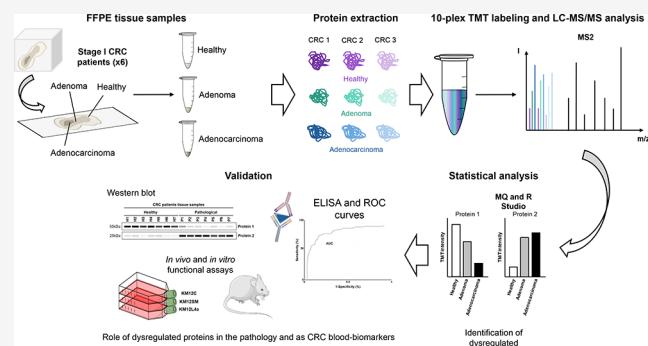
Metrics & More

Article Recommendations

Supporting Information

**ABSTRACT:** A deeper understanding of colorectal cancer (CRC) biology would help to identify specific early diagnostic markers. Here, we conducted quantitative proteomics on FFPE healthy, adenoma, and adenocarcinoma tissue samples from six stage I sporadic CRC patients to identify dysregulated proteins during early CRC development. Two independent quantitative 10-plex TMT experiments were separately performed. After protein extraction, trypsin digestion, and labeling, proteins were identified and quantified by using a Q Exactive mass spectrometer. A total of 2681 proteins were identified and quantified after data analysis and bioinformatics with MaxQuant and the R program. Among them, 284 and 280 proteins showed significant upregulation and downregulation (expression ratio  $\geq 1.5$  or  $\leq 0.67$ ,  $p$ -value  $\leq 0.05$ ), respectively, in adenoma and/or adenocarcinoma compared to healthy tissue. Ten dysregulated proteins were selected to study their role in CRC by WB, IHC, TMA, and ELISA using tissue and plasma samples from CRC patients, individuals with premalignant colorectal lesions (adenomas), and healthy individuals. *In vitro* loss-of-function cell-based assays and *in vivo* experiments using three CRC cell lines with different metastatic properties assessed the important roles of SLC8A1 and TXNDC17 in CRC and liver metastasis. Additionally, SLC8A1 and TXNDC17 protein levels in plasma possessed the diagnostic ability of early CRC stages.

**KEYWORDS:** colorectal cancer, quantitative proteomics, TMT, FFPE tissue, SLC8A1, TXNDC17



## INTRODUCTION

Colorectal cancer (CRC) development is a complex process in which histological, morphological, genetic, epigenetic, and proteomics changes accumulate and lead to tumor progression from polyps (adenomas) to adenocarcinomas.<sup>1,2</sup> CRC is the third most common cancer type and the second cause of cancer-related death worldwide.<sup>3,4</sup> More than 60% of CRC patients are diagnosed at late stages, stages III and IV, when cancer cells have already colonized other organs and the 5-year survival rate drops to 70 and 10%, respectively.<sup>5</sup> Most tumor alterations, such as mutations in APC, KRAS, or TP53 genes and their effect on protein functions and cellular processes are well characterized.<sup>6,7</sup> However, a better understanding of the biology of the disease in its initial steps would allow the identification of potential markers of cancer development parallel to the progression of the disease that could be used to improve the clinical management of CRC patients.

CRC carcinogenesis has been described as a multistep process involving four stages. At stages I and II, tumor cells are limited to the large bowel, whereas at stages III and IV they

spread to neighboring or distal tissues, respectively, mainly lymphatic nodes, lungs, and liver.<sup>1,7</sup> Furthermore, the ecosystem in which CRC cells are embedded is modified during cancer progression by tumor cells to form the tumor microenvironment (TME). The TME is as complex and heterogeneous as cancer cells, and it is associated with cancer recurrence, metastasis, and drug resistance.<sup>8–10</sup> Thus, the study of CRC tissue samples encompassing cancer cells and tumor stroma, which is missed by the analysis of CRC cells in culture, is relevant to gain insight into cancer development.<sup>11</sup>

Different proteomics techniques have been used to study molecular pathways related to CRC,<sup>12,13</sup> as well as to identify diagnostic markers for the early detection of the dis-

Received: November 9, 2023

Revised: September 24, 2024

Accepted: October 10, 2024

Published: October 23, 2024

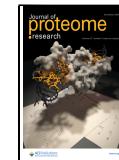


**Table 1.** Tissue and Plasma Samples from Healthy Individuals, Individuals with Premalignant Lesions, and CRC Patients Used in the Study

samples	number (n)	age average $\pm$ SD (years)	age range (years)	Gender (n)		CRC stage (n)			
				male	female	I	II	III	IV
Tissue Samples									
TMT-1	paired <sup>a</sup>	3	73 $\pm$ 6	67–78	2	1	3		
TMT-2	paired <sup>a</sup>	3	70 $\pm$ 9	60–78	1	2	3		
WB	paired <sup>a</sup>	7	77 $\pm$ 8	65–87	5	2	1	2	2
Plasma Samples									
healthy individuals		32	58 $\pm$ 10	24–74	15	17			
premalignant lesions		10	65 $\pm$ 10	49–79	8	2			
CRC patients		38	75 $\pm$ 9	56–88	22	16	10	10	11
									7

<sup>a</sup>Adenoma, adenocarcinoma, and healthy FFPE paired tissues or healthy and adenocarcinoma OCT paired tissues.

ease.<sup>11,14–16</sup> Remarkably, quantitative mass spectrometry is conceived as an interesting tool for molecular, cellular, and system biology studies allowing for the identification and quantification of thousands of proteins with a high sensitivity and specificity, comparing simultaneously multiple samples in a single experiment.<sup>17–19</sup> Formalin-fixed paraffin-embedded tissue samples (FFPE) have become the best material for analysis in the clinical routine because (i) paraffin blocks maintain tissues' qualitative and quantitative properties and architecture for long periods of time, allowing, in combination with microdissection, for the precise and reproducible separation of local tissue regions, (ii) FFPE is the standard protocol for tissue processing in pathological routine diagnostics worldwide since the late 1800s, and (iii) FFPE tissues are intrinsically linked to clinical records and might be associated with additional pathological data, such as genomics or immunohistochemistry.<sup>20–22</sup>

Here, we aimed at studying protein dysregulation in CRC by quantitative proteomics using microdissected FFPE tissues from paired healthy, original adenoma, and surrounding colorectal adenocarcinoma tissues from six sporadic CRC patients (stage I), unrelated to either p53 alterations or microsatellite instability, to account for interpatient and intertissue variations in the analysis.<sup>23</sup> More than 2500 proteins were identified and quantified using a Q Exactive Orbitrap mass spectrometer, analyzing separately paired adenoma, adenocarcinoma, and healthy tissues in two TMT10-plex experiments. Among them, 566 proteins showed dysregulation throughout tumor progression in comparison to controls (1.5-expression ratio), identifying both proteins previously related to CRC and novel interesting potential markers of the disease. After data analysis, ten proteins were selected by extensive bioinformatics and meta-analysis to study their association with CRC and their role as markers for diagnosis and prognosis by Western blot (WB), immunohistochemistry (IHC) using specific CRC tissue microarrays (TMA), and ELISA using paired tissue and plasma samples from CRC patients at different stages, individuals with premalignant lesions (low- and high-grade adenomas), and individuals with negative colonoscopy (controls). Additionally, transient silencing of SLC8A1 and TXNDC17 performed in three isogenic CRC cell lines with different metastatic properties allowed us to determine their association with CRC metastasis to the liver. Finally, quantification of SLC8A1 and TXNDC17 protein levels by ELISA in plasma showed potential as early blood-based diagnostic biomarkers of CRC.

## METHODS

### Human Samples

The Institutional Ethical Review Boards of the Instituto de Salud Carlos III, and Hospital Clínico San Carlos (Madrid) approved this study on biomarker discovery and validation (CEI PI 13\_2020-v2). Tissue samples were obtained from the Hospital Clínico San Carlos (IdISSC) biobank, which belongs to the National Biobank Net (ISCI) and was cofounded with FEDER funds, after approval by the Ethical Review Boards of these institutions. Written informed consent was obtained from all patients. Tissue samples were collected using a standardized sample collection protocol and stored at  $-80^{\circ}\text{C}$  until use.<sup>24,25</sup> Adenocarcinoma tissue samples were classified based on international consensus criteria. Moreover, healthy tissue was the area of normal large bowel mucosa at the periphery of the polyp, where the crypt architecture was preserved with no dysplasia; whereas premalignant areas were foci of adenoma with low-grade dysplasia.

For mass spectrometry analysis, paired healthy, adenoma, and adenocarcinoma FFPE tissue samples from six CRC patients (stage I) obtained by laser microdissection were used (Tables 1 and S1). For WB analysis, paired healthy and tumoral optimal cutting temperature (OCT)-embedded frozen tissue samples from seven CRC patients at stages I–IV were used (Tables 1 and S1). Plasma samples used for ELISA tests included 32 samples from healthy individuals, 10 samples from individuals with premalignant lesions, and 38 samples from CRC patients at stages I–IV (Tables 1 and S2).

### Cell Models

For the analysis of the role of selected dysregulated proteins in metastasis, isogenic KM12C (RRID:CVCL\_9547), KM12SM (RRID:CVCL\_9548), and KM12L4a (RRID:CVCL\_W220) CRC cells, from I. Fidler's laboratory (MD Anderson Cancer Center) were used. KM12 cells were expanded in the laboratory to prepare a large batch of working aliquots that were stored in liquid nitrogen. For each experiment, cells were thawed and kept in culture for a maximum of 10 passages. These cell lines were not authenticated in our laboratory. Isogenic SW480 (RRID:CVCL\_0546) and SW620 (RRID:CVCL\_0547) CRC cells from the American Type Culture Collection (ATCC) cell repository were used.<sup>26–28</sup> These cell lines were authenticated by ATCC and were passaged after purchase for all of the experiments. CRC cells were cultured at  $37^{\circ}\text{C}$  and 5%  $\text{CO}_2$  in Dulbecco's Modified Eagle Medium (DMEM, Lonza, Basel) supplemented with 10% fetal bovine serum (FBS, Sigma-Aldrich), 1× L-glutamine

(Lonza), and 1× penicillin/streptomycin (Lonza), and continuously monitored for mycoplasma contamination.

#### Microdissection, Protein Extraction, and PAGE-SDS

Microdissection was guided by a pathologist specialist in the digestive system, who reviewed the paraffin block sections. Sections from paraffin blocks were cut at 10  $\mu\text{m}$  and wet-mounted on Zeiss PEN membrane slides (Zeiss) in a protease-free vessel with mass spectrometry grade H<sub>2</sub>O at 42 °C. The slide sections were dried completely for 2 h at 50 °C to prevent the sections from detaching from the slides during deparaffinization. Deparaffinized sections were then briefly stained with hematoxylin for 60 s, followed by two immediate washes with mass spectrometry grade H<sub>2</sub>O. Tissue sections were air-dried for 5 min, facing up on a paper towel, and used directly for microdissection. Otherwise stated, the sections were cut and captured in the laser microdissection system of the Leica DM6000B microscope (Leica Biosystems, Wetzlar, Germany), operated at energy 40, and cutting speed 10.

Then, pathological-guided microdissected FFPE tissues were transferred to 1.7 mL tube caps and deparaffinized by washing twice with 500  $\mu\text{L}$  heptane (Sigma-Aldrich) for 1 h at room temperature (RT) and 700 rpm.<sup>29</sup> Prior to centrifugation at 15,000g to collect tissues, 25  $\mu\text{L}$  of 100% methanol was added to each sample for tissue rehydration. Then, tissues were centrifuged and lysed with 300  $\mu\text{L}$  of lysis buffer (RIPA, Sigma-Aldrich) supplemented with 1× protease and phosphatase inhibitors (MedChemExpress) by manual disaggregation using 16G and 18G needle syringes until homogeneity was observed. Samples were then incubated at 700 rpm and 100 °C for 20 min and subsequently at 80 °C for 2 h to remove paraffin traces and revert cross-linking. Finally, samples were centrifuged at 10,000g and 4 °C for 10 min and protein extracts (supernatants) were collected and stored at -80 °C until use. About 50–100 mg of each FFPE tissue sample were used for deparaffination and protein extraction.

Protein extracts from OCT-embedded CRC tissue samples were obtained by cutting into small pieces on dry ice OCT tissues and washed twice with 500  $\mu\text{L}$  of PBS 1×, which was subsequently discarded by centrifugation at 10,000g and 4 °C for 5 min. Then, tissues were lysed with 500  $\mu\text{L}$  of RIPA supplemented with 1× protease and phosphatase inhibitors and mechanically disaggregated (2 cycles of 30 s at 30 Hz) using the TissueLyser II (Qiagen). Finally, samples were centrifuged at 10,000g and 4 °C for 10 min and protein extracts (supernatants) were collected and stored at -80 °C until use.

Proteins extracts from CRC cells were obtained after harvesting cells at 90% confluence with PBS 1× containing 4 mM EDTA (Carl Roth). Cells were lysed with 1000  $\mu\text{L}$  of RIPA supplemented with 1× protease and phosphatase inhibitors and manually disaggregated using 16G and 18G needle syringes until homogeneity was observed. After sample centrifugation at 10,000g and 4 °C for 10 min, protein extracts (supernatants) were collected and stored at -80 °C until use.

Protein concentration was determined by Trp quantification method,<sup>30</sup> and confirmed by Ponceau red staining of nitrocellulose membranes after 10% SDS-PAGE under reducing conditions.

#### 10-Plex TMT Labeling and Protein Fractionation

Two 10-plex TMT-based quantitative proteomics experiments were used to analyze protein dysregulation in paired healthy, adenoma, and adenocarcinoma FFPE tissue samples from six

different CRC patients (TMT-1: lot SG253267; TMT-2: lot TC264165; Thermo Fisher Scientific). For each experiment, paired healthy ( $n = 3$ ), adenoma ( $n = 3$ ), and adenocarcinoma ( $n = 3$ ) tissue samples were separately labeled.

In total, 8  $\mu\text{g}$  of each protein extract in 100  $\mu\text{L}$  of RIPA were reduced with 10  $\mu\text{L}$  of 100 mM tris(2-carboxyethyl)phosphine (TCEP, Sigma-Aldrich) for 45 min at 37 °C and 800 rpm and alkylated with 11  $\mu\text{L}$  of 0.4 M chloroacetamide (Sigma-Aldrich) for 30 min at RT and 800 rpm in the dark. Next, samples were incubated with 100  $\mu\text{L}$  of SeraMag magnetic beads mix (50% hydrophilic beads –50% hydrophobic beads, GE Healthcare) and 200  $\mu\text{L}$  of 100% acetonitrile (ACN) for 35 min at RT and 600 rpm to allow protein binding to the beads. Then, supernatants were discarded, and the magnetic beads were washed twice with 70% ethanol and once with 100% ACN. Finally, supernatants were discarded, and proteins were digested overnight (o/n) at 37 °C and 800 rpm with 0.4  $\mu\text{g}$  of porcine trypsin (Thermo Fisher Scientific) in 100  $\mu\text{L}$  of 200 mM HEPES at pH 8.0. The next day, the samples were sonicated, and the supernatant was collected. Beads were sonicated again with 100  $\mu\text{L}$  of 200 mM HEPES (pH, 8.0) to ensure peptide recovery, and the two supernatants per experiment were pooled together. In each experiment, all peptides from the 9 samples were separately labeled with 0.4 mg of each Tandem Mass Tags reagent (Thermo Fisher Scientific) according to the manufacturer's instructions. Briefly, the 0.8 mg of each TMT reagent that covalently labels primary amines of Lys and the N-termini of trypsin-digested peptides were resuspended in 41  $\mu\text{L}$  of 100% ACN. Samples were incubated first with 10  $\mu\text{L}$  of the corresponding reagent for 30 min at 600 rpm and RT, followed by a second incubation with 10  $\mu\text{L}$  of the same reagents for 30 min at 600 rpm and RT. After TMT labeling and to quench the reaction, samples were incubated with 10  $\mu\text{L}$  of 1 M glycine 30 min at 600 rpm and RT. Finally, the content of the 9 tubes was pooled together and dried under vacuum prior to separation using a High pH Reversed-Phase Peptide Fractionation Kit (Pierce). Briefly, desiccated peptide samples were reconstituted in 300  $\mu\text{L}$  H<sub>2</sub>O, 0.1% trifluoroacetic acid (TFA), applied to the columns, and peptides were separated in 12 fractions of 300  $\mu\text{L}$  each in a triethylamine-ACN gradient (2.5–100% ACN).<sup>31,32</sup> Fractions were then mixed in six fractions,<sup>33</sup> which were directly dried under vacuum and stored at -80 °C until LC-MS/MS analysis using a Q Exactive mass spectrometer (Thermo Fisher Scientific).

#### LC-MS/MS Analysis

Samples were resuspended in 10  $\mu\text{L}$  of 0.1% formic acid (FA) and 4  $\mu\text{L}$  of each sample were injected per run. Peptide separation was carried out on an Easy-nLC 1000 nano system (Thermo Fisher Scientific). For each analysis, samples were loaded into a precolumn Acclaim PepMap 100 (Thermo Fisher Scientific) and eluted in an RSLC PepMap C18, 50 cm long, 75  $\mu\text{m}$  inner diameter, and 2  $\mu\text{m}$  particle size (Thermo Fisher Scientific). The mobile phase flow rate was 300 nL/min using 0.1% FA in water (solvent A) and 0.1% FA in 100% ACN (solvent B). The gradient profile was set as follows: 3–7% solvent B for 5 min, 7–25% solvent B for 95 min, 25–60% solvent B for 14 min, 60–95% solvent B for 1 min, and 100% solvent B for 8 min.

For ionization, 1900 V of liquid junction voltage and 250 °C capillary temperature were used. The full scan method employed a *m/z* 300–1800 mass selection, an Orbitrap

resolution of 70,000 (at  $m/z$  200), a target automatic gain control (AGC) value of  $3 \times 10^6$ , and maximum injection times (IT) of 100 ms. After the survey scan, the 15 most intense precursor ions were selected for MS/MS fragmentation. Fragmentation was performed with a normalized collision energy (NCE) of 27 and MS/MS scans were acquired with a starting mass of  $m/z$  100, AGC target of  $1 \times 10^5$ , resolution of 35,000 (at  $m/z$  200), intensity threshold of  $2 \times 10^4$ , isolation window of 1.6  $m/z$  units, and maximum IT of 100 ms. Charge state screening was enabled to reject unassigned, singly charged, and more than or equal to seven protonated ions. A dynamic exclusion time of 30 s was used to discriminate between previously selected ions.

### MS Data Analysis

MS data were analyzed with MaxQuant (version 1.6.6.0) using standardized workflows. Mass spectra \*.raw files were searched against Uniprot UP000005640\_9606.fasta *Homo sapiens* (human) 2019 database (20962 protein entries) using the Reporter ion MS2 type. TMT10 was specified as a variable modification on lysine and peptide N-termini. Precursor and reporter mass tolerance were set to 4.5 ppm and 0.003 Da, respectively, allowing 2 missed cleavages. Carbamidomethylation of cysteines was set as a fixed modification, and methionine oxidation and acetylation N-terminal were set as variable modifications. Additionally, although neither phosphopeptide enrichment nor phosphoproteomics analysis was performed, Ser, Thr, and Tyr phosphorylation was also set as variable modifications. Reporter ion intensities were bias-corrected for the overlapping isotope contributions from the TMT tags according to the manufacturer's certificate. Unique and Razor peptides were considered for quantification. Minimal peptide length and maximal peptide mass were fixed to 7 amino acids and 4600 Da, respectively, and identified peptides were filtered by their precursor intensity fraction (PIF) with a false discovery rate (FDR) threshold of 0.01. The protein sequence coverage was estimated for specific proteins by the percentage of matching amino acids from the identified peptides having confidence greater than or equal to 95% divided by the total number of amino acids in the sequence. The mass spectrometry proteomics data have been deposited to the ProteomeXchange Consortium via the PRIDE partner repository with the data set identifier PXD039630.<sup>34</sup>

### Bioinformatic Analysis

Heatmaps of the  $\log_2$  expression ratios (Fold change, FC) of dysregulated proteins were obtained with MultiExperiment Viewer (MeV, version 4.9.0), and row data normalization was performed for better data visualization. Proteins identified as dysregulated in adenoma and/or adenocarcinoma tissues in comparison to healthy tissues were then analyzed with STRING (version 11.0) and Reactome Pathway databases to study the protein enrichment and to identify the altered networks and pathways in which these proteins are involved.<sup>35</sup> STRING settings were fixed to MCL clustering enrichment 2 and 0.4 confidence score.

In addition, an extensive meta-analysis of selected proteins was performed by analyzing whether genetic alterations and dysregulations had been previously described them as associated with CRC. To this end, the c-Bioportal database was used,<sup>36</sup> which gives information about genetic alterations identified in tumor tissue samples.

### Western Blot

The protein content of tissue samples and CRC cells was analyzed by WB using 10  $\mu$ g of each protein extract separated on 10% SDS-PAGE under reducing conditions and transferred to nitrocellulose membranes at 100 V for 2 h. Then, membranes were blocked with 0.1% Tween PBS 1 $\times$  supplemented with 3% skimmed milk (blocking buffer) during 1 h at RT and incubated with primary antibodies at optimized dilutions (Table S4) in blocking buffer O/N at 4 °C. Then, membranes were washed 3 times with 0.1% Tween PBS 1 $\times$  and incubated with the appropriate indicated HRP-conjugated secondary antibodies (Table S4) diluted in blocking buffer for 1 h at RT. Next, membranes were washed 3 times with 0.1% Tween PBS 1 $\times$ , and finally, the signal was developed using the SuperSignal West Pico PLUS Chemiluminescent Substrate (Thermo Fisher Scientific) and detected on an Amersham Imager 680 (GE Healthcare). Protein intensities were quantified using ImageJ software and normalized according to the total protein content of each line as observed using Ponceau red staining. GAPDH was used as the control in the assay.

### Immunohistochemistry and Tissue Microarrays

IHC staining was conducted in two TMAs containing (i) 55 cores from nonrecurrence CRC and 28 cores from recurrence CRC at stage II of the disease and (ii) 24 cores from nonmetastatic CRC samples and 19 cores from liver metastasis tissue samples. Slides were deparaffinized by incubation at 60 °C. Biopsies were cut and incubated with PT-Link (Dako) for 20 min at 95 °C in a pH-buffered solution. To block endogenous peroxidase, holders were incubated with the peroxidase-blocking reagent (Dako). Biopsies were stained for 20 min with the corresponding antibody at optimized dilution (Table S4) followed by incubation with the corresponding HRP-conjugated secondary antibody. Sections were then visualized with 3,3'-diaminobenzidine for 5 min and counterstained with hematoxylin. Immunoreactivity was graded as 0, absent; 1, mild staining; 2, moderate staining; or 3, intense staining. Cases were classified according to total staining (intensity of the staining per percentage of areas showing the reaction). In addition, slides were incubated with the HRP-conjugated secondary antibody as the negative control, which confirmed the absence of a background signal. TMAs were scanned with the NanoZoomer scanner (Hamamatsu photonics), and 40 $\times$  images were processed with NDP.view 2 software (version 2.7.2S).

### ELISA

ELISA tests were performed to quantify SLC8A1 and TXNDC17 levels in the plasma of patients in comparison with healthy individuals using commercial ELISA kits (ELH-TRP14, RayBio, and orb562227, Biorbyt) according to the manufacturer's instructions. Briefly, 96-well plates coated with the corresponding antibody were incubated with individual plasma samples (1:10 diluted) from CRC patients at stages I–IV ( $n = 38$ ), individuals with premalignant lesions ( $n = 10$ ), and healthy individuals ( $n = 32$ ). Then, plates were incubated with the HRP-conjugated reagent, and the color was developed according to the manufacturer's instructions. Finally, the colorimetric signal was read at 450 nm using The Spark multimode microplate reader (Tecan Trading AG).

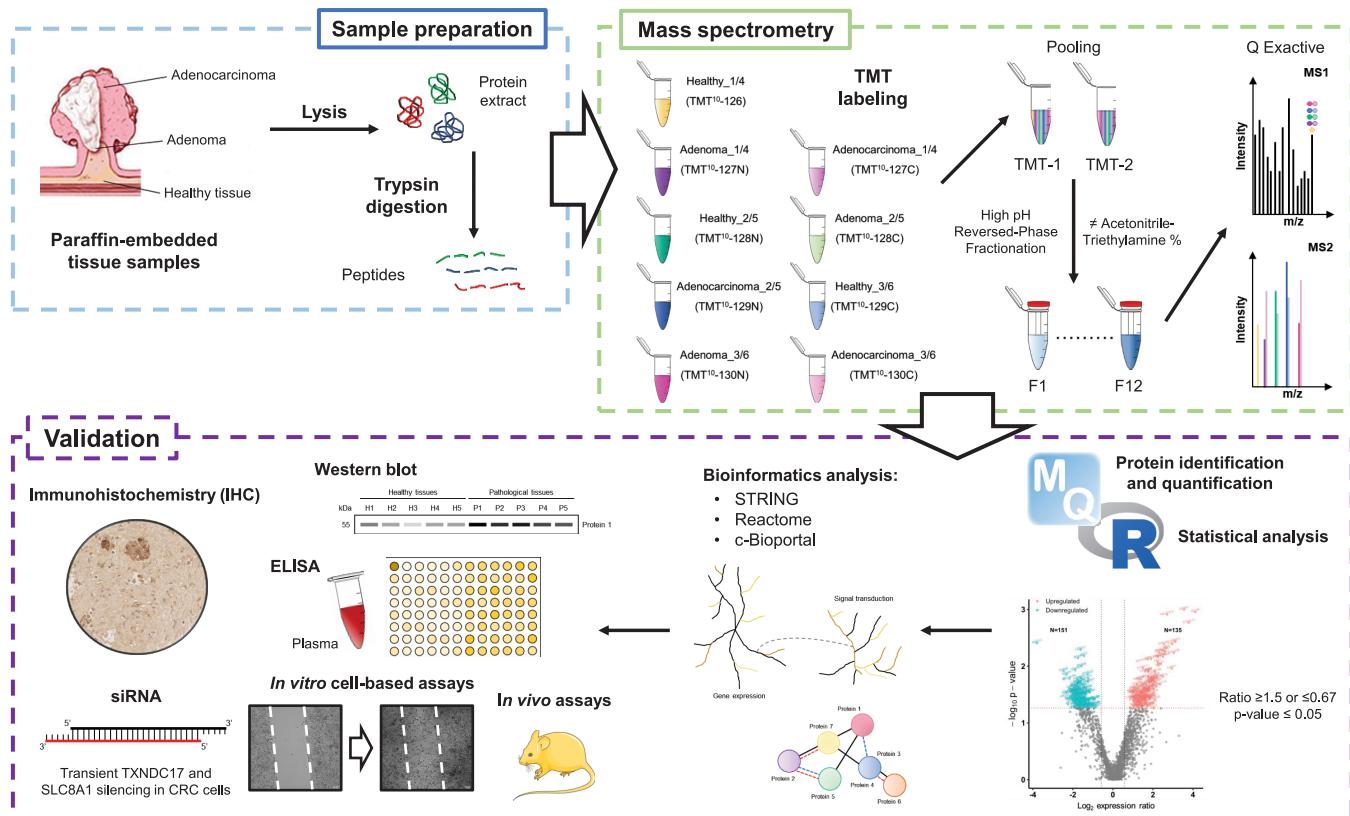


**Figure 1.** Workflow for the identification of dysregulated proteins in FFPE colorectal tissues by proteomics. Protein extracts from six sporadic CRC stage I patient tissue samples (paired FFPE healthy, adenoma, and adenocarcinoma samples) were trypsin digested, labeled with 18 different TMT reagents (two 10-plex TMT kits), and analyzed by LC-MS/MS using a Q Exactive Orbitrap mass spectrometer. Differences in protein levels between pathological (adenoma or adenocarcinoma) samples and adjacent healthy tissues were analyzed using MaxQuant and the R program. Meta-analysis of the 566 proteins selected as more prone to be associated with CRC ( $\geq 0.58$ -fold change, or  $\leq -0.58$ -fold change, and  $p\text{-value} \leq 0.05$ ) was subsequently performed using STRING and Reactome databases. Finally, ten proteins up- or downregulated in adenoma and/or adenocarcinoma were selected to get further insights into their role in the progression of the disease by WB, IHC, ELISA, and *in vitro* and *in vivo* experiments.

### Transient TXNDC17 and SLC8A1 Silencing

Transient silencing of TXNDC17 and SLC8A1 was achieved using the jetPRIME reagent (PolyPlus Transfection) with, alternatively, siTXNDC17 (EHU104981, Sigma-Aldrich), siSLC8A1 (EHU084891, Sigma-Aldrich) or control siRNAs (SIC001; Sigma-Aldrich), according to previous protocols in 6-well plates.<sup>37,38</sup> Forty-eight h after transfection, cells were analyzed by semiquantitative PCR or WB. Alternatively, 24 h after transfection cells were used for proliferation, adhesion, invasion, or wound healing loss-of-function assays and for *in vivo* homing experiments, as previously described.<sup>32,37–39</sup> *In vitro* assays were performed in duplicate, whereas *in vivo* assays were performed in quadruplicate.

### In Vivo Homing Experiments

The Ethical Committee of the Instituto de Salud Carlos III (Spain) approved the protocols used for the experimental work with mice after approval by the OEBA ethical committee (Proex 285/19).

For the analysis of the effect of TXNDC17 and SLC8A1 in *in vivo* liver homing, transient silencing of KM12SM cells was performed according to established protocols.<sup>38,39</sup> Then,  $1 \times 10^6$  KM12SM cells were intrasplenically injected in nude mice ( $n = 4$ ) in 0.1 mL of PBS 1× 24 h after transient silencing. Finally, 24 h after cell inoculation, mice were euthanized, and the RNA from the liver was isolated using TRIzol Reagent.

### RNA Extraction, cDNA Synthesis, Semiquantitative PCR, and qRT-PCR

CRC cells were harvested with trypsin-EDTA (Lonza) and RNA extracted with TRIzol-chloroform and purified using the RNeasy Mini Kit (Qiagen Inc.) according to the manufacturer's protocol. Mice tissues were incubated in TRIzol-chloroform, lysed with TissueLyser II (Qiagen), and RNA purified with the RNeasy Mini Kit (Qiagen Inc.). RNA quantification was performed with a NanoDrop 2000C instrument (Thermo Fisher Scientific). Next, 1  $\mu$ g of RNA was used to synthesize cDNA using the NZY First-Strand cDNA Synthesis Kit (NZYtech), according to manufacturers' instructions, and 0.8  $\mu$ L of cDNA was directly used for semiquantitative PCR and/or qRT-PCR analysis using TXNDC17 (Fw: CGCTTACTTTACGGGTTCTAAGG; Rv: GGCTTTCTCCTACTTGGCAGTA), SLC8A1 (Fw: G A G G C G A C C T C T T C C T G A T C G ; Rv: TCCGTTCCCTCCACGCTAGTA), 18S (Fw: ACCCGTTGAACCCCATTCTGTGA; Rv: GCCTCACTAAC-CATCCAATCGG), and human GAPDH (hGAPDH, Fw: CGGCCATCACGCCACAGTTTC; Rv: GGCTGAAACGGGAAGCTTGT), and murine  $\beta$ -Actin (m $\beta$ Actin, Fw: C A T G T A C G T A G C C A T C C A G G C ; Rv: CTCTTTGATGTCACGCACGAT) specific oligonucleotides.

qRT-PCR was performed with a Light Cycler 480 (Roche) (50 cycles at 55 °C) using the TB Green Premix Ex TaqII

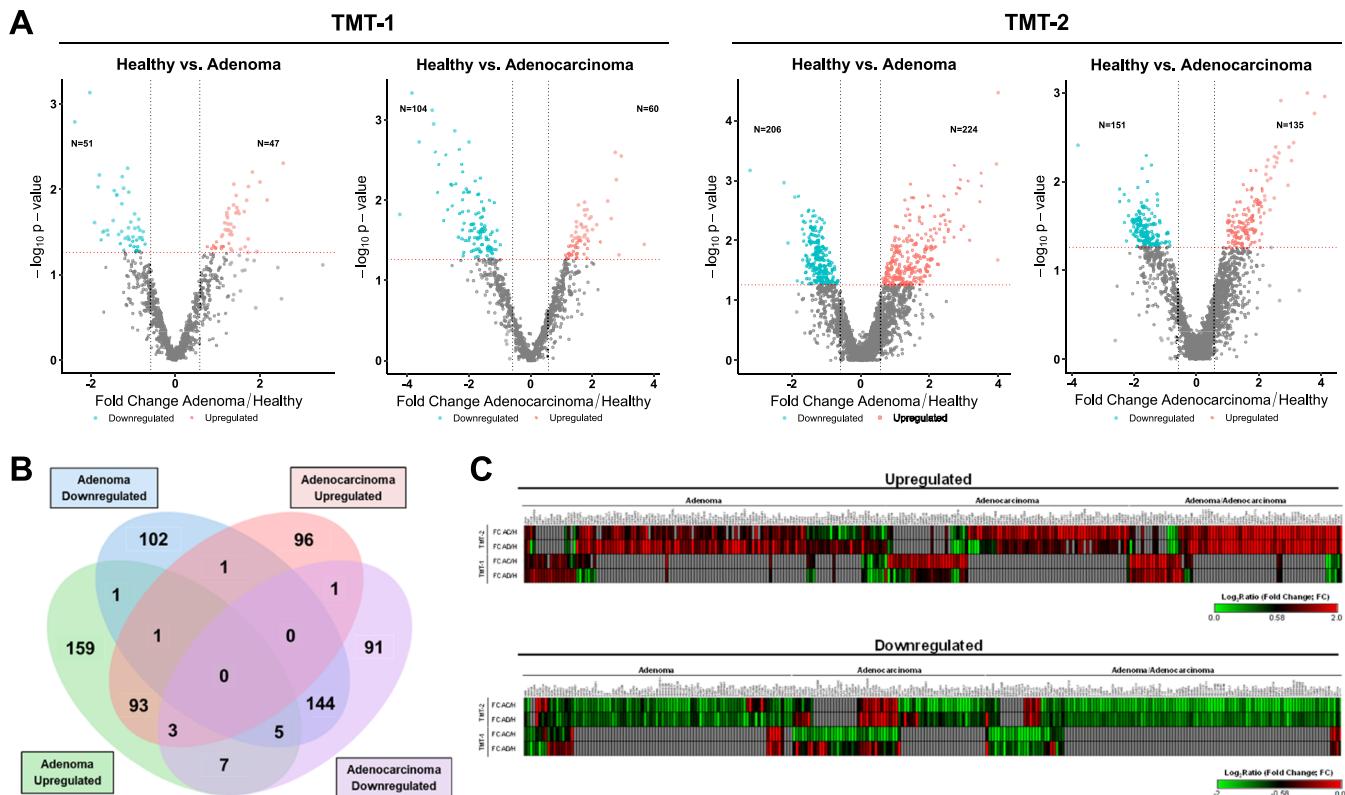


**Figure 2.** Differential analysis of the proteins identified and quantified from the two 10-plex TMT experiments using paired FFPE healthy, adenoma, and adenocarcinoma tissue samples. (A) Volcano plots of proteins identified and quantified as altered in adenoma or adenocarcinoma in comparison to healthy tissues in both TMT experiments. The *x*-axis represents the  $\log_2$  expression ratio (fold change –FC–) of protein expression differences between adenoma/adenocarcinoma and healthy samples; the *y*-axis depicts the *p*-value based on  $-\log_{10}$ . Colored dots represent differentially expressed proteins upregulated (red) and downregulated (green) in pathological tissues with *p*-value  $\leq 0.05$  (*p*-value = 0.05 represented by red dashed horizontal line) and 1.5-fold expression difference (represented by two black dashed vertical lines). (B) Venn diagram of the 704 proteins dysregulated in adenoma or adenocarcinoma tissues in comparison to adjacent healthy paired tissue with a  $\geq 0.58$  or  $\leq -0.58$ -fold change expression difference and *p*-value  $\leq 0.05$ . (C) Heatmaps of the FC obtained for the 566 proteins identified as dysregulated in adenoma and/or adenocarcinoma tissues, including HIPK1 and APPL1. Green: downregulated proteins; Red: upregulated proteins. H: Healthy; AD: Adenoma; AC: Adenocarcinoma.

(Takara) and the corresponding above-indicated specific oligonucleotides.<sup>37,38</sup> mRNA levels were used for normalization. Relative gene expression was calculated using the  $2^{-\Delta\Delta Ct}$  method.<sup>32,38</sup>

#### Statistical Analysis

Plots, mean, and standard deviation (SD) of the WB, IHC, and ELISA analyses were performed with Microsoft Excel 2019 and GraphPad Prims 5 programs.

Student's *t* test values were calculated with Microsoft Excel 2019 after confirming by the F-test that the two sample groups were homoscedastic. One-tailed was used for the statistical analysis. *p*-values  $\leq 0.05$  were considered statistically significant. ROC curves (Receiver Operating Characteristic Curve) of each protein individually or in combination were constructed with R (version 3.6.2) using the "ModelGood" and the "Epi" packages. Venn diagram was obtained from the jvenn Web site (<http://bioinfo.genotoul.fr/jvenn>).<sup>40</sup>

## RESULTS

In this study, a quantitative TMT proteomics analysis of FFPE tissue samples from CRC patients was performed to identify dysregulated proteins associated with the adenoma–adenocarcinoma transition in CRC. For their identification, two 10-plex TMT experiments were performed using paired healthy,

adenoma, and adenocarcinoma FFPE tissue samples from six sporadic stage I CRC patients (Table 1). Proteins identified and quantified as dysregulated in the disease were further investigated *in vitro* and *in vivo* to analyze their role in CRC development and progression. A workflow of the study is depicted in Figure 1.

#### Identification of Proteins Dysregulated in CRC by LC-MS/MS

Dissected FFPE tissue samples from six sporadic CRC patients were analyzed by mass spectrometry to identify and quantify dysregulated proteins during the adenoma–adenocarcinoma transition in CRC. After tissue lysis, 8  $\mu$ g of each healthy (*n* = 6), adenoma (*n* = 6), and adenocarcinoma (*n* = 6) protein extracts were trypsin digested, labeled with different TMT reagents separately, and analyzed by LC-MS/MS using a Q Exactive mass spectrometer.

First, as the same amount of protein was labeled with each TMT reagent, differences in the total sum of signals of each channel were corrected by computing normalization factors to equal these sums. Thus, sample loading (SL) and Trimmed Mean of M-values (TMM) normalizations were carried out with R Studio (version 4.1.1) according to an established protocol (<https://github.com/pwilmart>), using "tidyverse", "psych", "gridExtra", "scales", and "ggplot2" packages (Figure

**Table 2.** Selected Dysregulated CRC-Associated Proteins for Validation and Further Analysis

protein ID	protein name	gene name	tissue of dysregulation	dysregulation
Q9UKG1	DCC-interacting protein 13- $\alpha$	APPL1	adenoma/adenocarcinoma	downregulated
P14209	CD99 antigen	CD99	adenocarcinoma	downregulated
Q9BPU6	dihydropyrimidinase-related protein 5	DPYSL5	adenoma/adenocarcinoma	downregulated
Q86Z02	homeodomain-interacting protein kinase 1	HIPK1	adenoma/adenocarcinoma	downregulated
Q9P1Y6	PHD and RING finger domain-containing protein 1	PHRF1	adenoma	downregulated
P78324	tyrosine-protein phosphatase nonreceptor type substrate 1	SIRPA	adenoma	downregulated
Q9UJW0	dynactin subunit 4	DCTN4	adenoma	upregulated
P24844	myosin regulatory light polypeptide 9	MYL9	adenoma	upregulated
P32418	sodium/calcium exchanger 1	SLC8A1	adenoma/adenocarcinoma	upregulated
Q9BRA2	thioredoxin domain-containing protein 17	TXNDC17	adenoma/adenocarcinoma	upregulated

**S1).**<sup>41</sup> After data normalization, 2681 proteins were identified and quantified with at least one unique peptide and an ion score above 99% in the two TMT analyses, with 682 proteins in common between both TMT experiments (924 proteins were identified and quantified in TMT-1 and 2439 proteins were identified and quantified in TMT-2). Proteins identified as potential contaminants were excluded from the analysis. Due to the different depths in the proteome and the poor overlap between both TMT experiments, we decided to analyze them separately for the identification of dysregulated proteins associated with CRC. Next, sample clustering was determined by principal component analysis (PCA) using the “stats” R package prior to statistical analysis to investigate the variability of the biological replicates. Samples named Healthy\_2, Healthy\_4, and Adenocarcinoma\_3 clustered separately from their corresponding groups, most probably because of interindividual biological variability, and were omitted for the identification and analysis of dysregulated proteins (Figure S2a). After data analysis, a moderated t-statistical analysis was performed with R Studio (version 4.1.1) using the packages “dplyr”, “limma”, “edgeR”, and “rstatix” after data filtering (proteins identified in at least 30% of samples were considered for the analysis) and missing value imputation by random draws from a Gaussian, using the “imputeLCMD” R package. Proteins identified with one or more unique peptides, an expression ratio  $\geq 1.5$  or  $\leq 0.67$ , and  $p\text{-value} \leq 0.05$  were selected as statistically adenoma or adenocarcinoma upregulated or downregulated, respectively, proteins (Table S3 and Figure 2A).

From the two TMT experiments, a total of 693 proteins showed dysregulation in adenoma and/or adenocarcinoma, without considering 11 proteins showing a statistically significant conflicting opposite dysregulation, upregulated in one TMT and downregulated in the other TMT- in both TMT experiments (Figure 2B and Table S3).

Among the total of 693 dysregulated proteins identified and quantified, we found proteins dysregulated in colorectal adenoma or adenocarcinoma or dysregulated in the same direction in both pathological tissues (348 upregulated and 337 downregulated proteins) in comparison to healthy adjacent tissues. In addition, eight dysregulated proteins showed an opposite dysregulation between adenoma and adenocarcinoma tissue samples, suggesting that these proteins might regulate the proliferation of cancer cells and the development of the pathology (Figure 2B and Table S3). Interestingly, some of these proteins had been previously described as altered in CRC, such as CDH17 or ITGB4,<sup>12,25,42,43</sup> supporting the reliability of the assays for the identification of dysregulated proteins associated with the

adenoma–adenocarcinoma transition in CRC; even though TMT experiments were analyzed separately.

Finally, a total of 121 proteins showing statistical significant dysregulation in one TMT and a conflicting nonstatistical opposite dysregulation in the other TMT (expression ratio  $\geq 1.5$ —upregulated and  $\leq 0.67$ —downregulated) were omitted in further subsequent analysis (Table S3 and Figure S2b,c). Thus, 284 upregulated and 280 downregulated proteins significantly associated with the disease were used in the following analyses (Figure 2C and Table S3). Interestingly, most of the proteins found statistically dysregulated in adenoma tissues, except eight, showed a similar dysregulation in the same direction in adenocarcinoma samples and *viceversa*, suggesting a key role of these proteins in the development and progression of CRC. In addition, two nonstatistically highly downregulated proteins (HIPK1 and APPL1) were also included in subsequent analyses (Table S3). HIPK1 was previously related to CRC as a tumor suppressor or promoter of the disease in a stage-dependent manner.<sup>44</sup> APPL1 was observed to play a key role in several processes closely related to CRC, such as cell proliferation, survival, or apoptosis. It is also related to the insulin-signaling pathway, type II diabetes mellitus (DM) being one of the main risk factors for CRC.<sup>39,45</sup>

### Bioinformatics Analysis of Proteins Altered in CRC

Next, these 566 dysregulated proteins in adenoma and/or adenocarcinoma tissues were investigated using STRING and Reactome databases. First, significantly dysregulated pathways involving most of the downregulated and upregulated proteins in CRC were found with Reactome, highlighting Complement cascade (46/156 proteins, FDR =  $7.66 \times 10^{-15}$ ), Immune system (119/2661 proteins, FDR =  $4.65 \times 10^{-15}$ ), Translation (29/339 proteins, FDR =  $8.34 \times 10^{-08}$ ), Regulation of apoptosis (14/55 proteins, FDR =  $1.11 \times 10^{-08}$ ), rRNA processing (26/247 proteins, FDR =  $9.46 \times 10^{-09}$ ), Regulation of RAS by GAPS (15/71 proteins, FDR =  $1.64 \times 10^{-08}$ ), Metabolism of proteins (79/2238 proteins, FDR =  $8.41 \times 10^{-05}$ ), Deubiquitination (22/289 proteins, FDR =  $7.63 \times 10^{-06}$ ), Cellular response to stimuli (53/1051 proteins, FDR =  $3.09 \times 10^{-07}$ ), Interleukin-1 signaling (16/125 proteins, FDR =  $4.78 \times 10^{-07}$ ), and MAPK6/MAPK4 signaling (17/106 proteins, FDR =  $2.69 \times 10^{-08}$ ) (Figure S3). Furthermore, using STRING more than 20 different significant clusters of direct and indirect interactions among proteins ( $FDR < 0.02$ ) were obtained for upregulated and downregulated proteins (Figure S4a). Remarkably, these clusters revealed protein networks related to CRC, such as metabolic processes, signaling pathways, gene expression, cell adhesion, immune response, cytoskeleton organization, or transport.

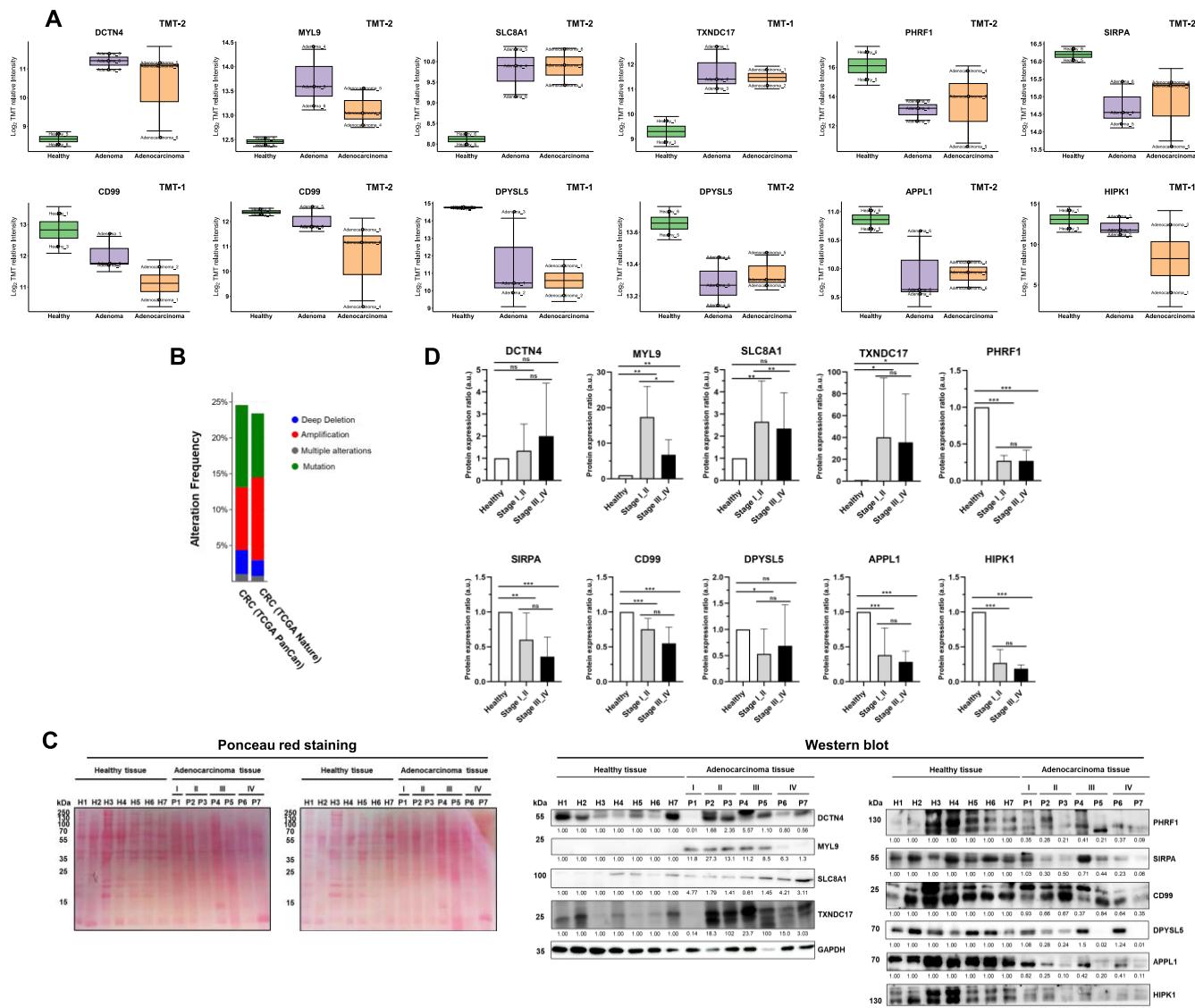


**Figure 3.** Validation of LC-MS/MS data. (A) Graph bar representing the mean and standard deviation (SD) of the Log<sub>2</sub> TMT relative intensities obtained by mass spectrometry of the 10 proteins upregulated and downregulated selected for validation, in adenoma or adenocarcinoma tissues in comparison to healthy tissue samples. (B) c-Bioportal analysis revealed genetic alterations associated with CRC (TCGA Nature 2012 and PanCancer Atlas) in the 10 selected proteins. (C) WB analysis of OCT-embedded paired healthy and tumoral tissue samples from 7 CRC patients at stages I–IV. Protein level differences between paired pathological and healthy tissues are shown, most of these proteins are statistically significant dysregulated in patients. (D) Protein band intensities obtained by WB were quantified by densitometry using ImageJ and normalized according to the total protein content of each line as observed by Ponceau red staining. GAPDH was used as the control in the assays. ns: nonsignificant; \*: p-value <0.05, \*\*: p-value <0.01, \*\*\*: p-value <0.001; a.u.: arbitrary units. Mean and SD are represented in the graph bars.

Collectively, most of these networks and pathways were expected to be altered in CRC, supporting the obtained results. The processes identified here, in which dysregulated proteins associated with CRC are involved, might be altered during the progression of the disease and thus might be of further interest for the study of the development and progression of CRC.

After bioinformatics analysis, we selected 10 out of the 566 proteins for validation and confirmation of their dysregulation during tumor progression and to determine their relevance for the development of the disease, according to (i) existing information about their association with CRC or other cancers, (ii) the biological processes, functions, and cellular localizations of the dysregulated proteins, prioritizing those processes closely related to CRC, and (iii) proteins showing dysregulation in adenoma or adenocarcinoma tissues and their

expression ratio (higher expression ratios were preferred). Proteins dysregulated in both adenoma and adenocarcinoma tissues were mainly chosen (APPL1, DPYSL5, SLC8A1, and TXND17), with two of them (CD99 and HIPK1) showing a dysregulation associated with the progression of the disease, suggesting that the dysregulation of these proteins is associated with colorectal cancer development and progression (Table 2 and Figure 3A). For the other proteins selected but for MYL9, although nonsignificant, the expression levels of these proteins in adenoma (CD99) or adenocarcinoma (DCTN4, PHRF1, and SIRPA) were also higher (DCTN4) or lower (CD99, PHRF1, and SIRPA) than those in the paired healthy tissues. Regarding MYL9, the dysregulation was found only in adenoma tissues, whereas little differences were observed in adenocarcinoma tissue samples. Finally, the analysis with c-

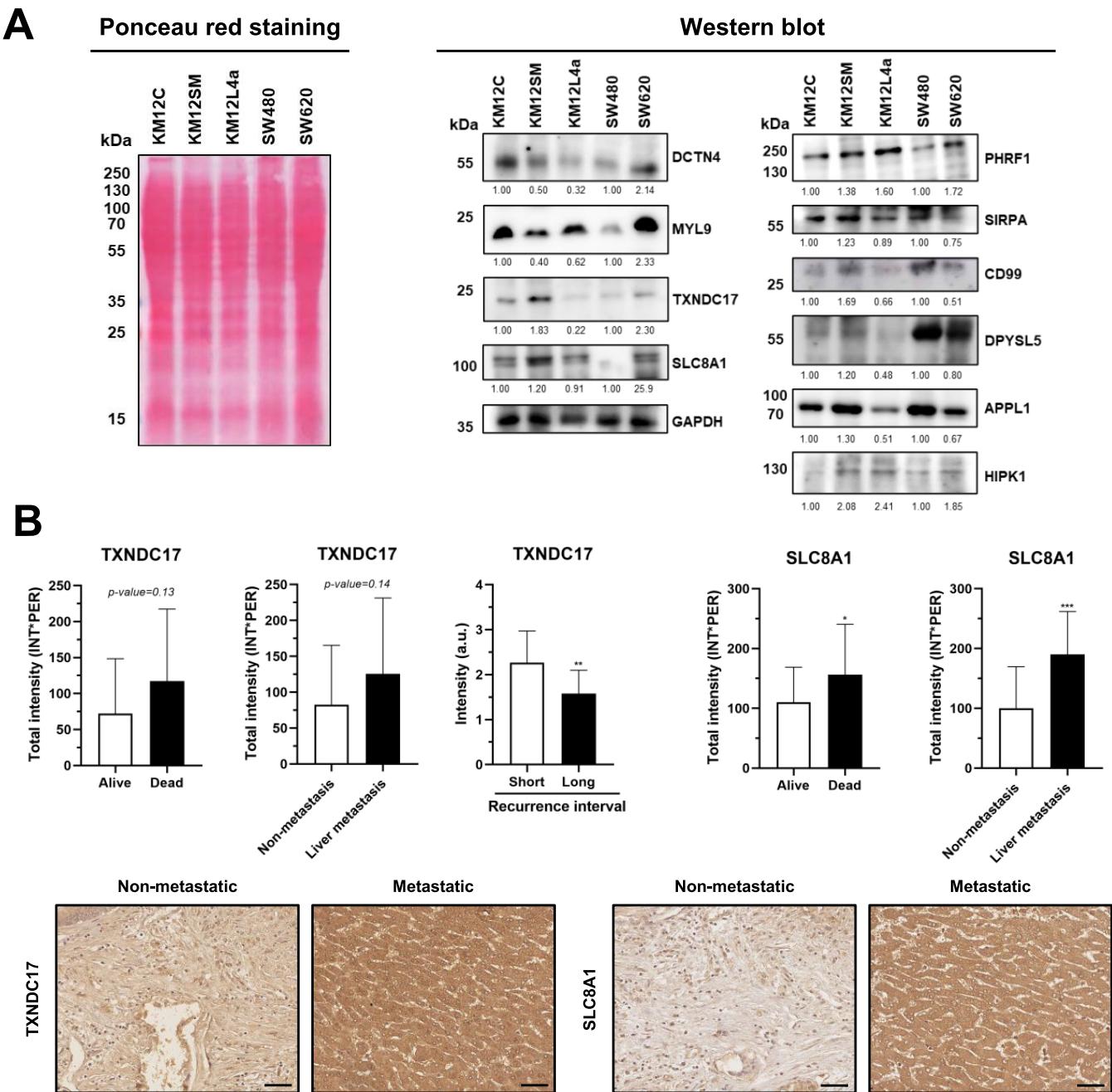


**Figure 4.** Analysis of the role of dysregulated proteins in CRC metastasis. (A) Western blot analysis of 5 CRC cell lines with low (KM12C and SW480) and high (KM12SM, KM12L4a, and SW620) metastatic capacities. Differences at the protein level were observed for most of the dysregulated proteins associated with the metastatic capacity of CRC cells to the liver, lung, or lymphatic nodes. Band quantifications were performed relative to the nonmetastatic (KM12C or SW480) isogenic cells. (B) TMA results confirmed the association of high TXND17 and SLC8A1 protein levels with the worst CRC prognosis and metastasis to the liver, and the association of TXND17 overexpression with CRC recurrence. Representative images of the TXND17 and SLC8A1 staining of the liver and nonliver metastasis and recurrence and nonrecurrence stage II CRC patients are shown. Scale bar: 50  $\mu$ m. For WB, GAPDH was used as the control in the assays, whereas protein band intensities were quantified by densitometry using ImageJ and normalized according to the total protein content of each line as observed by Ponceau red staining. ns: nonsignificant; \*:  $p$ -value  $<0.05$ , \*\*:  $p$ -value  $<0.01$ , \*\*\*:  $p$ -value  $<0.001$ ; a.u.: arbitrary units. Mean and SD are represented in the graph bars.

Bioportal of the 10 selected proteins showed different genetic alterations for all of them, previously described in more than 20% of the CRC cases registered in The Cancer Genome Atlas (TCGA) (Figure 3B), supporting the hypothesis that these proteins might be involved in tumor development. The role of these ten proteins in tumor progression was then studied by WB, IHC, and ELISA using tissue and plasma samples from CRC patients at different stages of the disease.

#### Analysis of Protein Levels During Tumor Progression

The association of the ten selected proteins with CRC was confirmed by WB analysis using an independent cohort of adenocarcinoma tissue samples from CRC patients at different stages of the disease (stage I–IV) and paired healthy adjacent tissues. DCTN4, MYL9, SLC8A1, and TXND17 proteins were observed to be upregulated in adenocarcinoma in comparison with healthy adjacent tissue, whereas APPL1,

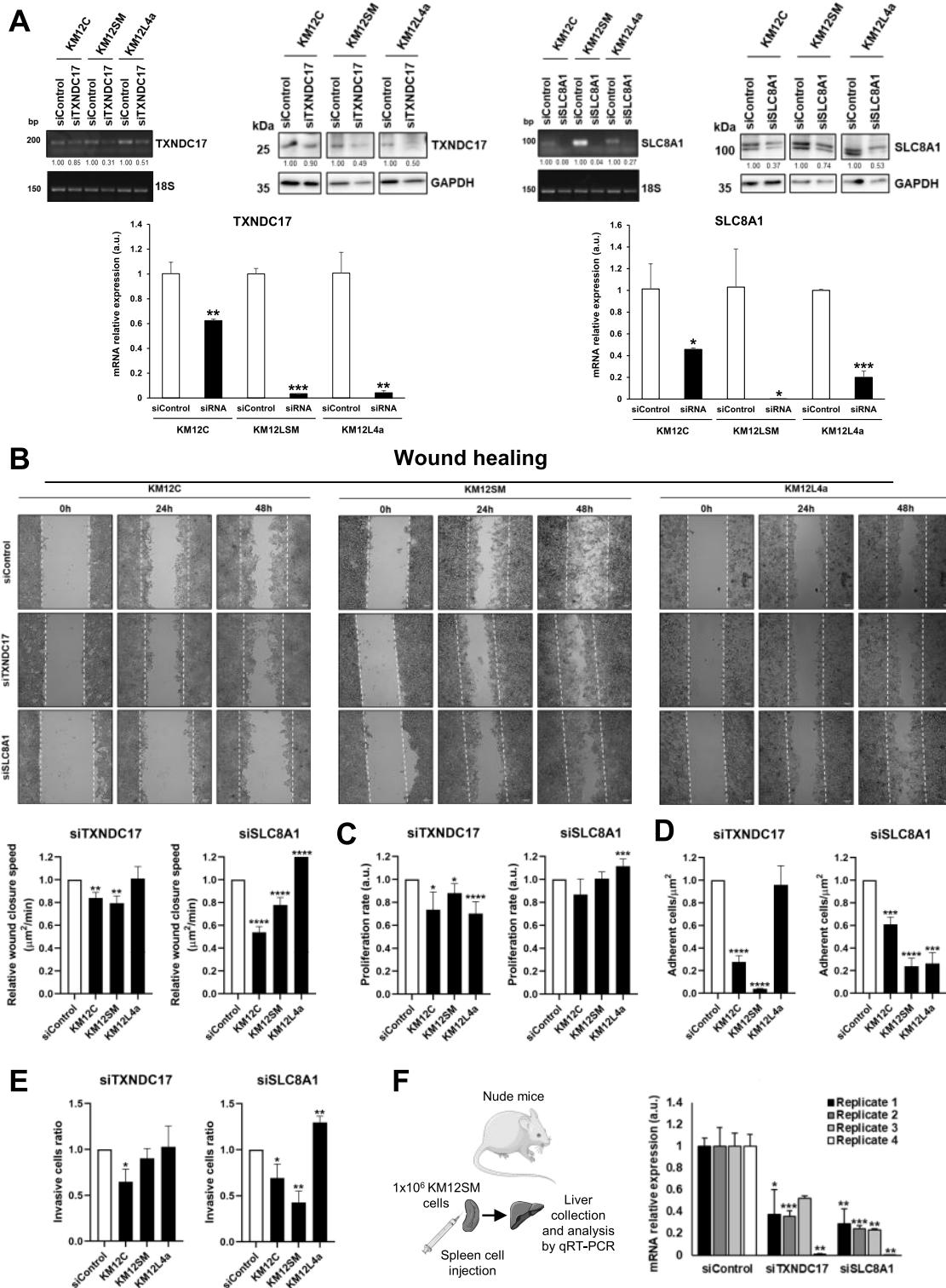


**Figure 5.** Functional analysis of TXNDC17 and SLC8A1 to evaluate their role in CRC progression and metastasis. (A) PCR and WB confirmed the depletion of both proteins in KM12C, KM12SM, and KM12L4a cells upon transient silencing. (B) *In vitro* wound healing assay revealed a major effect of SLC8A1 and TXNDC17 in KM12SM and KM12C cells than in KM12L4a, suggesting an association of both proteins with liver metastasis. (C) *In vitro* proliferation cell-based assay revealed a decrease in the proliferation capacity of KM12 cells upon TXNDC17 depletion, whereas no major effects were observed upon SLC8A1 depletion in the proliferation rate of KM12 cells. (D) *In vitro* adhesion assay revealed a major effect of SLC8A1 in the adhesive properties of KM12L4a, KM12SM, and KM12C CRC cells, whereas the depletion of TXNDC17 seemed to have no effect on KM12L4a cells in contrast to KM12SM and KM12C CRC cells. (E) *In vitro* invasion assay revealed a higher effect of SLC8A1 in the invasive properties of KM12 cells than TXNDC17. (F) *In vivo* homing experiments with nude mice and qRT-PCR analysis revealed a significant decrease in the number of KM12SM cells able to colonize the liver after TXNDC17 and SLC8A1 silencing, supporting previously observed effects on migration. \*:  $p$ -value  $<0.05$ ; \*\*:  $p$ -value  $<0.01$ ; \*\*\*:  $p$ -value  $<0.001$ ; \*\*\*\*:  $p$ -value  $<0.0001$ ; a.u.: arbitrary units. Mean and SD are represented in the graph bars.

CD99, DPYSL5, HIPK1, PHRF1, and SIRPA proteins were found to be downregulated in tumoral tissues, as previously observed by proteomics (**Figures 3C,D** and **S4b**). Although TMT and WB results were not 100% comparable due to the lack of premalignant tissues (low- and high-grade adenoma) in the WB, both techniques showed concordance in the dysregulation observed of selected proteins in the disease in comparison to healthy tissue samples. No differences in protein levels were observed for the candidate proteins according to the stage of the disease except for MYL9, whose expression was significantly higher in the early stages of the disease (**Figure 3C,D**), in concordance with the proteomics data.

Although for PHRF1, DCTN4, and SIRPA proteins the dysregulation found by proteomics was mainly associated with adenoma tissues, these proteins also showed by proteomics a high dysregulation in adenocarcinoma tissue (expression ratios  $>2.3$ , and  $p$ -values  $<0.1$ ), which is in agreement and concordant with the results obtained by WB at different stages of the disease.

Regarding CD99, this protein was found significantly downregulated in adenocarcinoma tissues, and by WB we could confirm the downregulation of this protein in adenocarcinoma. In addition, although nonsignificant, we could observe a trend of a decrease of the levels of this protein with the stage of the disease. Finally, regarding MYL9, this protein was mainly found upregulated in adenoma tissue samples compared to adenocarcinoma tissue by proteomics, and by WB we could observe significantly higher levels of this protein at early stages of the disease, thus confirming the significant dysregulation of this protein at the beginning of the disease and in adenoma tissues. These results suggest the potential role of these proteins and the biological pathways in which they are involved in CRC progression.

Further investigation of the role of the selected proteins in CRC metastasis was achieved by analyzing their protein expression in five isogenic CRC cell lines with low (KM12C and SW480) and high (KM12SM—liver tropism, KM12L4a—liver and lung tropism, and SW620—lymphatic node tropism) metastatic abilities. HIPK1 and PHRF1 expression levels were increased in the three metastatic cells, indicating that these proteins might be involved in CRC progression and metastasis (**Figure 4A**). In addition, the other dysregulated proteins seemed to be related to metastatic tropism. In this sense, overexpression of APPL1, CD99, DPYSL5, SIRPA, SLC8A1, and TXNDC17 was associated with KM12SM CRC cells (liver tropism), whereas downregulation of APPL1, CD99, DCTN4, DPYSL5, MYL9, SIRPA, and TXNDC17 correlated with KM12L4a CRC cells (liver and lung tropism). On the other hand, higher protein levels of DCTN4, MYL9, TXNDC17, and SLC8A1 and lower levels of APPL1, CD99, DPYSL5, and SIRPA were associated with SW620 CRC cells (lymphatic node tropism) (**Figure 4A**).

SLC8A1 and TXNDC17 have not been previously associated with CRC and were found here differentially expressed in CRC patients and associated with liver tropism (upregulated in KM12SM and downregulated in KM12L4a CRC cells). Thus, we further investigated the dysregulation of SLC8A1 and TXNDC17 in tissue samples from CRC patients by IHC. Two TMAs were used to analyze the role of both proteins in CRC liver metastasis, survival, and recurrence. Interestingly, SLC8A1 and TXNDC17 were found upregulated in liver metastasis, and higher levels of both proteins were associated with a worse prognosis of the disease (**Figure 4B**).

Finally, higher levels of TXNDC17 significantly correlated with shorter (cutoff 2.46 years) recurrence intervals (**Figure 4B**). These data suggest a potential role of SLC8A1 and TXNDC17 in CRC progression and liver metastasis.

### Role of TXNDC17 and SLC8A1 in CRC Liver-Associated Metastasis

Then, the role of SLC8A1 and TXNDC17 in the tumorigenic and metastatic abilities of CRC cells and in CRC liver metastasis was investigated *in vitro* and *in vivo* using the KM12 cell model of CRC metastasis.<sup>12,26,27,32,38,39</sup> *In vitro* cell-based assays (proliferation, adhesion, invasion, and wound healing) and *in vivo* experiments were performed 24 h after transient depletion of SLC8A1 and TXNDC17 proteins with specific siRNAs (**Figure 5**).

For transient transfection,  $2.5 \times 10^5$  cells were incubated with 22 pmol of each siRNA using 2  $\mu$ L of JetPRIME Transfection reagent and 100  $\mu$ L of JetPRIME buffer. Then, the depletion of TXNDC17 and SLC8A1 was confirmed at mRNA and protein level by semiquantitative PCR, qRT-PCR, and WB (**Figure 5A**). Higher depletion levels were observed in KM12SM and KM12L4a metastatic CRC cells. Then, the wound closure ability of KM12 CRC cells was analyzed after transient SLC8A1 and TXNDC17 depletion (**Figure 5B**). A statistically significant reduction in the migration capacity of the KM12C and KM12SM siTXNDC17 and siSLC8A1 CRC cells was observed. On the contrary, depletion of SLC8A1 significantly increased the migration capability of KM12L4a cells, whereas TXNDC17 depletion did not affect KM12L4a metastatic capacities. Next, the proliferative and adhesive properties of the KM12 cell system upon TXNDC17 and SLC8A1 depletion was assessed (**Figure 5C,D**). The proliferation capacity of KM12C, KM12SM, and KM12L4a cells was reduced upon TXNDC17 transient silencing, whereas the proliferation capacity of KM12 cells was barely affected upon SLC8A1 transient depletion (**Figure 5C**). Indeed, upon SLC8A1 depletion, the proliferation ability of KM12C and KM12L4a cells was nonsignificantly reduced and significantly increased, respectively, with KM12SM cells almost unaffected. Moreover, the depletion of TXNDC17 and SLC8A1 produced a significant and major reduction of the adhesive properties of KM12C and KM12SM CRC cells. In KM12L4a CRC cells, SLC8A1 depletion significantly reduced its adhesive properties, in contrast to TXNDC17 that did not produce any change in the adhesion capacity of these cells (**Figure 5D**). Additionally, a significant decrease in the invasion capacity of SLC8A1 transiently silenced KM12C and KM12SM cells was observed, with major effects, about 2-fold decrease, on KM12SM liver metastatic CRC cells. For KM12L4a cells, a significant 25% increase was observed. In contrast, TXNDC17 significantly induced a decrease in the invasion of KM12C cells, with almost no effect on KM12SM and KM12L4a cells (**Figure 5E**).

Previous WB results pointed out an association of SLC8A1 and TXNDC17 to liver metastasis, and *in vitro* migration, proliferation, adhesion, and invasion cell-based assays upon depletion of both proteins also suggested that major effects on metastatic cells took place on liver metastatic KM12SM CRC cells, with inconclusive results on liver and lung metastatic KM12L4a CRC cells. Thus, we hypothesized that SLC8A1 and TXNDC17 could play a role *in vivo* in the liver metastasis of CRC cells. To address this question, *in vivo* homing experiments ( $n = 4$ ) were performed with KM12SM cells upon transient siRNA silencing of both proteins, separately, in

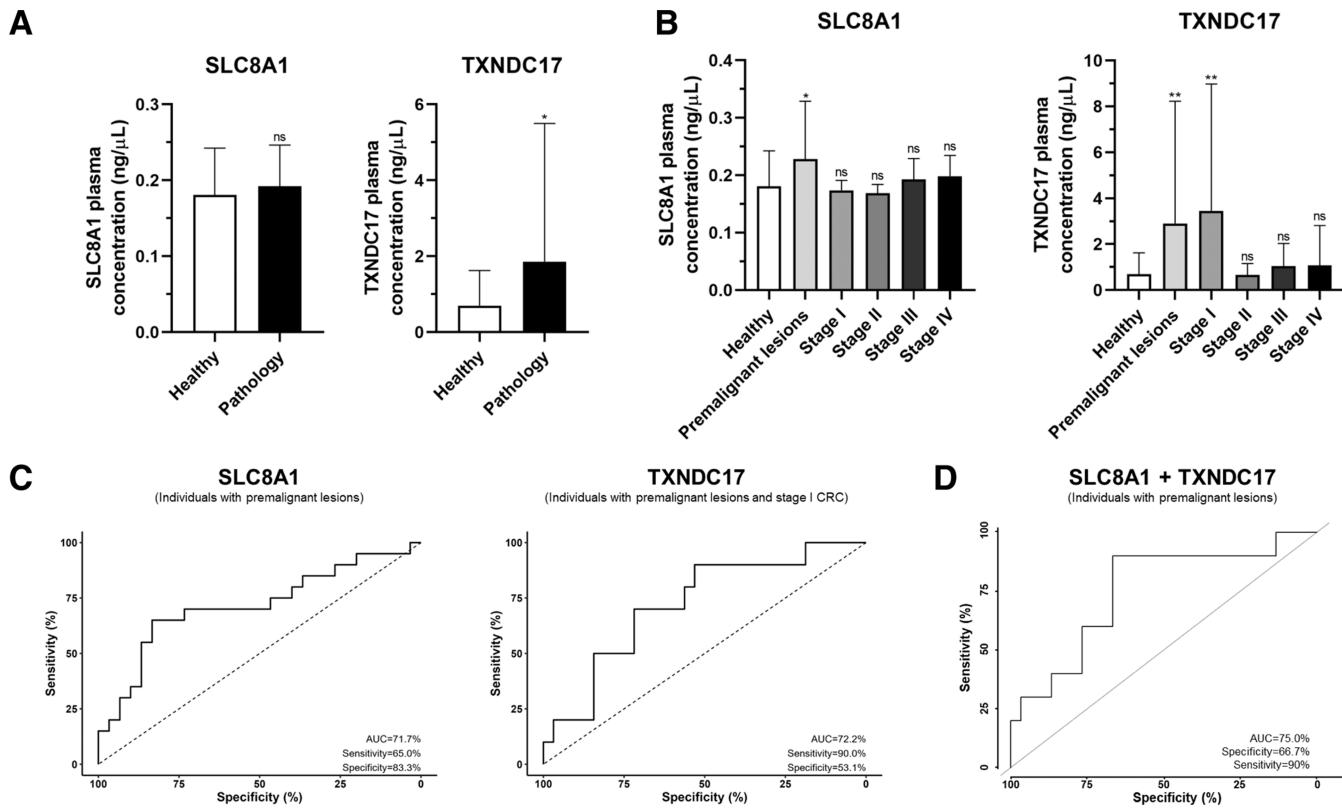


**Figure 6.** Quantification of SLC8A1 and TXNDC17 plasma levels in CRC patients, individuals with colorectal premalignant lesions, and healthy individuals by ELISA. (A) Graph bar of the plasma concentration of SLC8A1 and TXNDC17 in individuals with premalignant lesions and CRC patients (pathology group), and healthy individuals. Higher levels of TXNDC17 were significantly associated with CRC. No differences were found for SLC8A1. (B) Graph bar of SLC8A1 and TXNDC17 plasma levels according to the stage of the disease. Higher plasma levels of both proteins were significantly associated with individuals with premalignant lesions and CRC patients at stage I. (C) ROC curve analyses revealed a high diagnostic ability of both proteins at the early stages of the disease. An individual AUC higher than 70% was obtained for both proteins, with a sensitivity and specificity higher than 65%. (D) The two proteins in combination showed a high potential for the detection of premalignant individuals and CRC patients at early stages of the disease, with a ROC curve showing an AUC of 75.0%, a sensitivity of 90%, and a specificity of 66.7%. ns: nonsignificant; \*:  $p$ -value <0.05, \*\*:  $p$ -value <0.01. Mean and SD are represented in the graph bars.

comparison to the siRNA control. As a surrogate marker for the presence of KM12SM cells on murine livers after 24 h of spleen cell inoculation (and 48 h post-transfection), human GAPDH was amplified by qRT-PCR, using murine  $\beta$ -Actin as control of the assays (Figure 5F). The transient depletion of both proteins induced a statistically significant, except in one replicate of TXNDC17, decrease in the liver homing ability of KM12SM metastatic cells of about 55% for TXNDC17 and 70% for SLC8A1 in four independent *in vivo* experiments in comparison with control siRNA-transfected KM12SM cells.

Collectively, our results, in agreement with the dysregulation of these proteins in liver metastatic cells, demonstrate the role of SLC8A1 and TXNDC17 in CRC progression and liver metastasis.

#### SLC8A1 and TXNDC17 Protein Levels in Plasma Showed Diagnostic Ability of CRC

Finally, the potential role of SLC8A1 and TXNDC17 as blood-based biomarkers of autoimmune diseases was investigated. To this end, we analyzed by ELISA the abundance of both proteins in plasma from individuals with premalignant lesions ( $n = 10$ ) and CRC patients at stages I–IV ( $n = 38$ ) in comparison to healthy individuals ( $n = 32$ ). The abundance of the protein TXNDC17 in plasma was found significantly higher in patients (individuals with premalignant lesions and CRC patients) than in healthy individuals whereas no

differences were observed for SLC8A1 (Figure 6A). Interestingly, we found statistically significant higher levels of TXNDC17 in individuals with premalignant lesions and CRC patients at stage I of the disease, whereas the abundance of TXNDC17 in plasma of CRC patients at stages II–IV were not significantly different from that of healthy individuals (Figure 6B). These results suggest an increased accumulation of TXNDC17 in CRC cells at advanced stages of the disease, as observed by WB. Regarding SLC8A1, a higher plasma abundance of SLC8A1 was significantly found in individuals with premalignant lesions in comparison to healthy individuals (Figure 6B).

Finally, ROC curves were obtained to elucidate the potential diagnostic ability of quantification of the abundance of TXNDC17 and SLC8A1 in plasma (Figure 6C). As differences in plasma concentration of SLC8A1 and TXNDC17 were found in individuals with premalignant lesions and individuals with premalignant lesions and CRC patients at stage I, respectively, ROC curves were generated to evaluate these data in comparison with healthy individuals. Both proteins showed an area under the curve (AUC) higher than 70%, with a sensitivity and specificity higher than 65%, which demonstrates the usefulness of the determination of the concentration in plasma of both proteins for the detection of individuals with premalignant lesions and CRC patients at stage I. Finally, since both proteins demonstrated diagnostic potential for individuals

with colorectal premalignant lesions, we conducted ROC curve analyses using SLC8A1 and TXNDC17 together to assess their combined diagnostic ability (**Figure 6D**). The combination of both proteins showed a high diagnostic ability of individuals with premalignant lesions, with an AUC of 75%, and sensitivity and specificity higher than 65%.

Collectively, the analysis of FFPE adenoma, adenocarcinoma, and healthy paired tissues by TMT quantitative proteomics and validation by orthogonal techniques, using CRC cells and OCT-frozen paired healthy/tumoral tissues from CRC patients, confirmed the dysregulation of proteins not previously associated with CRC, with an interesting value of SLC8A1 and TXNDC17 as early blood-based biomarkers of the disease and with a key role in CRC progression and metastasis, as confirmed by *in vitro* and *in vivo* analysis using murine models of metastasis mimicking CRC liver homing colonization.

## ■ DISCUSSION

Despite years of research in CRC and important increases in life expectancy after diagnosis, CRC is still the second leading cause of cancer-related death worldwide. Most patients are still diagnosed at advanced stages of the disease (stages III and IV), when surgery is not enough and chemotherapy and/or radiotherapy are needed.

Proteomics studies offer a high and deep knowledge about cancer biology, as they provide information about tumor protein profiles that can allow the identification of diagnostic and prognostic biomarkers, as well as therapeutic targets of intervention.<sup>46</sup> Different proteomics studies have been performed for the identification of CRC-associated biomarkers,<sup>47</sup> with studies based on 2D-gels and mass spectrometry,<sup>48–50</sup> DIA (data independent acquisition),<sup>51,52</sup> or SILAC, TMT, and iTRAQ experiments,<sup>53–56</sup> using both CRC cell lines or human samples (tissues or plasma samples from patients and healthy individuals). Our work complements these investigations on CRC protein dysregulation to try to identify dysregulated proteins associated with the adenoma–adenocarcinoma transition. Here, we have analyzed FFPE-paired healthy, adenoma, and stage I adenocarcinoma tissue samples from CRC patients by TMT10-plex quantitative proteomics to identify proteins involved in the early onset and progression of CRC. Additionally, we were able to identify the processes in which most of the dysregulated proteins were involved, such as immunity, apoptosis, metabolism, or signaling. Because these processes are mainly dysregulated in CRC cells during cancer progression, they might be key for further study of the disease. In contrast to other proteomics studies, such as DIA or LFQ (label-free quantification) that require long data acquisition times for the analysis of 9 samples, another advantage of this work is that only 24 h of data acquisition was required for the simultaneous analysis of up to 10 tissue samples per experiment.

Although tissue samples are an enriched source of biomarkers, and their analysis allows the simultaneous study of cancer cells and TME, their high complexity might hamper biomarker discovery, due to intratumor and interindividual heterogeneity, and due to protein expression heterogeneity along the large bowel, even in healthy tissues.<sup>50</sup> Here, to reduce and minimize this variability, samples clustering separately by PCA from their respective groups due to biological interindividual heterogeneity were excluded from the subsequent statistical analysis. Additionally, the two TMT

experiments were analyzed separately due to important differences in proteome depth, primarily attributed to sample collection and processing, as well as to the stochasticity of the data-dependent acquisition (DDA) mass spectrometry technique used for the analysis (the 12 more intense peptides were randomly selected in each MS2 analysis). Moreover, microdissection of healthy, adenoma, and adenocarcinoma tissues included both the neoplastic cells and the stroma, and thus differences in the microdissected areas and the amount of stroma could have also contributed to the differences observed between both TMTs. Additionally, two different TMT kit lots were employed without a reference channel in the TMT experiments, which did not allow the combination and normalization of the two TMT experiments for the analysis. Therefore, to enhance the result reliability, proteins identified in both TMT experiments with conflicting opposite dysregulation ratios were omitted in subsequent analyses. Thus, 121 proteins showing statistically significant dysregulation between adenoma and adenocarcinoma in one TMT and conflicted nonsignificant opposite dysregulation in the other TMT were also omitted in subsequent analyses. Most of these proteins are commonly expressed in digestive glands and the gastrointestinal tract, particularly in the rectum and colon. Interestingly, only 18 of them have been previously associated with colonic cancer cells, suggesting that the observed opposite dysregulation of these proteins may stem from interindividual heterogeneity among the colorectal cancer samples involved in the study rather than from disease-related factors.

In this study, we have used early stage pathological tissue samples for discovery proteomics to identify proteins associated with early detection of the disease with biomarker potential. After bioinformatics analysis, selected candidate proteins were validated to elucidate their potential role in CRC. By proteomics, all candidate proteins were found dysregulated in both adenoma and adenocarcinoma tissues, highlighting CD99 and HIPK1, whose dysregulation was associated with the progression of the disease. Then, validation of protein dysregulation was performed by WB using a different cohort of paired healthy and pathological tissue samples from CRC patients. Upregulation and downregulation of the four and six candidate proteins, respectively, in adenocarcinoma in comparison with healthy tissues were confirmed. Interestingly, DCTN4 and SLC8A1, and CD99 and SIRPA protein levels increased or decreased, respectively, according to the progression of the disease, suggesting that these proteins, or the pathways associated with them, might have a key role in CRC progression. Furthermore, MYL9 protein levels were found upregulated mainly at the initial stages of CRC, highlighting the key role of this protein in the early onset of the disease. Finally, using five CRC cell lines with different metastatic abilities, we were able to find an association of the candidate proteins with CRC metastasis. Protein levels of PHRF1 and HIPK1 were found to be upregulated in the three metastatic CRC cell lines analyzed in comparison with the low metastatic isogenic controls. Because both proteins were found to be downregulated in adenoma and adenocarcinoma primary tumors, they might be involved in CRC metastasis, extravasation, invasion, and adhesion to the metastatic niche. In addition, the upregulation of APPL1, CD99, DPYSL5, SIRPA, SLC8A1, and TXNDC17 was associated with liver tropism of CRC cells, which was further confirmed for SLC8A1 and TXNDC17 *in vivo*.

Interestingly, some candidate proteins identified here as dysregulated in CRC have been previously related with CRC or other cancers, supporting the reliability of our approach for the identification of proteins associated with CRC, with CD99, DPYSL5, and APPL1 not previously associated with CRC, and TXNDC17 and SLC8A1 as novel proteins related to cancer, CRC, and/or CRC metastasis. DCTN4 (Dynactin subunit 4) is one of the 6 subunits that conform dynactin protein, which is required for cytoplasmic Dynein activity and, thus, is related to microtubules.<sup>57,58</sup> DCTN gene family have been described to have an important role in many cancers, and in several processes closely associated with the disease, such as cell cycle, apoptosis, or NF- $\kappa$ B signaling.<sup>59–63</sup> Although the function of DCTN4 has not been stated yet, this protein has been associated with low-grade glioblastomas,<sup>63</sup> and higher mRNA levels have been found in CRC primary tumors in comparison with paired healthy tissues.<sup>59</sup> Furthermore, DCTN4 has been described to be required for the expression of AHR (Aryl hydrocarbon receptor), which has been previously described as altered in CRC.<sup>32,64</sup> In addition, mRNA levels of DCTN4 were found to increase with the stage of CRC as we observed by proteomics analysis, which suggests a potential role of DCTN4 as a diagnostic and prognostic biomarker of CRC. Myosins have been strongly associated with tumor progression and metastasis.<sup>65</sup> Here, we identified MYL9 (myosin regulatory light polypeptide 9) as upregulated in CRC. This protein is involved in cytoskeleton dynamics, experimental metastasis, and invasion, and has been described as a tumor suppressor or an oncogene depending on the tumor type.<sup>66–70</sup> For CRC, MYL9 was previously found upregulated in CRC cells in comparison with normal human epithelium NCM460 cells, and involved in proliferation, migration, invasion, and angiogenesis.<sup>71</sup> In addition, high mRNA levels of MYL9 were found associated with early stages of CRC in patients, in concordance with our findings at the protein level.<sup>72</sup> Thus, we have validated here the association of MYL9 to the development and progression of CRC using human tissue samples and its association to the early stages of the disease and to the lymphatic nodes' tropism of cancer cells. PHRF1 (PHD and RING finger domain-containing protein 1) is a tumor suppressor reported as downregulated in several cancers, such as breast, lung, or leukemia, and also in CRC, as confirmed by our proteomics analysis.<sup>73–76</sup> However, PHRF1 overexpression has been associated with migration and invasion of lung cancer cells by modulating ZEB1 expression, which might support the association between PHRF1 overexpression and CRC metastasis reported in this study.<sup>77</sup> SIRPA (tyrosine-protein phosphatase nonreceptor type substrate 1) is a receptor-type transmembrane glycoprotein with an important role in cell–cell interaction.<sup>78</sup> CD99 (MIC2 or CD99 antigen) is a protein involved in cancer metastasis and inflammatory transendothelial migration, described as upregulated in some cancers, such as Ewing's Sarcoma and glioma.<sup>79,80</sup> However, a tumor suppressor-like activity of CD99 has also been described for other cancers, such as osteosarcoma.<sup>81</sup> According to our findings, CD99 protein is diminished in primary tumors and its expression is increased in CRC metastatic to liver cells, as shown by WB analysis and in concordance with other published data.<sup>80</sup> DPYSL5 (CRMP5 or dihydropyrimidinase-related protein 5) plays a major role in neural development and has been described as a regulator of proliferation and survival through the Notch-Akt signaling pathway in some cancers, such as glioblastoma or lung

cancer.<sup>82</sup> APPL1 (DCC-interacting protein 13- $\alpha$ ) has been described to promote the proliferation and metastasis of gastric cancer and other cancer cells by regulating STAT3, ERK1/2, and Akt2.<sup>83,84</sup> However, its role in the CRC has not been reported. We found this protein to be downregulated in colorectal primary tumors, whereas it was overexpressed in metastatic to liver CRC, suggesting a key role of this protein in CRC-associated metastasis, as previously described for other cancers. Finally, HIPK1 (homeodomain-interacting protein kinase 1) is a serine/threonine kinase that induces p53 and, consequently, p21 expression to decrease cell proliferation. In CRC, HIPK1 protein expression have been reported to diminish according to the stage of the disease, confirming our proteomics data.<sup>44</sup>

TXNDC17 (Thioredoxin domain-containing protein 17) is an oxidoreductase protein whose main function is to maintain cellular redox, thus regulating cell apoptosis, autophagy, and NF- $\kappa$ B signaling pathway.<sup>85,86</sup> Although there is not a clear association between TXNDC17 and cancer, it has been associated with chemoresistance in ovarian cancer, uterine papillary serous carcinoma, and chronic myeloid leukemia.<sup>87,88</sup> As this protein has been identified as overexpressed in CRC patients, it could also be involved in CRC chemoresistance. Finally, SLC8A1 (Sodium/calcium exchanger 1) regulates calcium reabsorption and homeostasis, which is related to cell proliferation and apoptosis.<sup>89</sup> Overexpression of SLC8A1 has been only related to papillary thyroid cancer progression.<sup>90</sup> Although no previous association between SLC8A1 protein levels and CRC has been reported, single-nucleotide polymorphisms (SNPs) and methylation alterations have been described to affect the SLC8A1 gene in CRC patients.<sup>89,91,92</sup> As TXNDC17 and SLC8A1 have not been previously related to CRC, and both proteins were found upregulated in primary tumors and associated with liver metastasis, further investigation was performed to elucidate their role in CRC-associated metastasis and as biomarkers of the disease. Both proteins were found associated with poor CRC survival, and TXNDC17 was also found associated with shorter recurrence time intervals by IHC, suggesting a potential role of both proteins as prognostic biomarkers of the disease. In addition, their association with liver metastasis was confirmed by IHC and by *in vitro* and *in vivo* assays after transient silencing of both genes in metastatic CRC cells. Finally, there is a clear need in CRC to identify blood-based diagnostic biomarkers because the only recommended clinical blood-based biomarker for CRC—carcinoembryonic antigen (CEA)—is not useful to detect early CRC due to significant overlap with benign disease, with sensitivities reaching 46% in recent studies,<sup>93,94</sup> we analyzed their potential as diagnostic biomarkers of CRC by ELISA. Both proteins were upregulated in the plasma of patients at initial stages of the disease, suggesting an interesting role of these proteins as early blood-based diagnostic biomarkers of CRC by liquid biopsy. Indeed, the measurement of plasma levels of SLC8A1 and TXNDC17 showed high diagnostic ability and sensitivity but lower specificity. Therefore, SLC8A1 and TXNDC17 should be useful for the detection of premalignant lesions and TXNDC17 should also be useful for early CRC detection through their analysis by a minimally invasive blood test. Whereas previous studies highlighted the ability of circulating methylated SLC8A1 DNA (ctDNA SLC8A1) to discriminate CRC patients at different stages of the disease from healthy individuals, TXNDC17 had not been previously described as a plasma

biomarker of CRC. However, the diagnostic capacity described for ctDNA SLC8A1 was lower (AUC: 58.9%; sensitivity: 45.8%; specificity: 73.2%) than that described here for SLC8A1 protein in plasma in CRC patients at early premalignant stages of the disease.<sup>95</sup> Accordingly, these proteins could be integrated into biomarker panels for the detection of CRC at early stages of the disease and specifically for the detection of premalignant lesions by a blood test either by ELISA, targeted proteomics (*i.e.*, PRM (parallel reaction monitoring)),<sup>96,97</sup> or by integrating the detection of different molecular markers in nature with electrochemical biosensors.<sup>96–99</sup> This latter approach could overcome limitations associated with lower specificity because biosensors offer greater limits of detection and limits of quantification for their measurement than other immunoassays.<sup>99,100</sup>

Finally, our study presents some limitations. First, in the discovery phase we used a limited number of sporadic CRC samples in stage I nonrelated to p53 mutations or microsatellite instability. Second, although we performed validation by different orthogonal techniques, further validation using a larger cohort of tissue and plasma samples from patients (primarily at the early stages of CRC) should be necessary to further confirm our results. Third, validation by other techniques, such as PRM or immunofluorescence, should complement the results obtained to validate the dysregulation of other proteins in plasma and tissue, respectively. Fourth, as proteomics analyses were performed using different lots of TMT reagents and because there was not so much overlap regarding the number of identified and quantified proteins in the two TMT experiments, statistical analysis was performed using a moderated *t* test, which is recommended for the analysis of a reduced number of samples per group, and both TMTs were analyzed separately. However, statistical analysis could have been enhanced if we had been able to normalize all of the samples simultaneously and consider all of the samples for strong statistical models. In this sense, after PCA analysis three samples that clustered separately from their counterparts probably due mostly to interindividual heterogeneity were omitted for statistical proteomics analyses and further consideration on subsequent analyses after proteomics. Furthermore, as many statistical tests were calculated, type-I errors could have been reduced by performing correction for multiple tests. Nevertheless, this would have supposed an increase in type II errors with the risk of missing potential novel biomarkers of CRC. Thus, correction for multiple tests was not performed, as the aim of this study was to identify and validate novel biomarkers by discovery proteomics and strong validation, as the latter was performed using a larger and different cohort of samples from CRC patients at different stages of the disease than in the proteomics experiments. Finally, although SLC8A1 and TXNDC17 protein levels in plasma and tissue samples were found higher in pathological samples than in healthy samples, we were unable to establish a direct correlation between their expression in tissue and plasma samples during the progression of the disease due to the lack of paired plasma and tissue samples from the same CRC patients.

## CONCLUSIONS

We have identified here by 10-plex TMT quantitative proteomics novel potential diagnostic and prognostic biomarkers of CRC associated with the development, progression, and metastasis of the disease. Validation performed by WB confirmed the dysregulation at the protein level of APPL1,

CD99, DCTN4, DPYSL5, HIPK1, MYL9, PRHF1, SIRPA, SLC8A1, and TXNDC17 in tumoral tissues in comparison with paired adjacent healthy tissues and in CRC cells with different metastatic abilities. In addition, further validation of the role of SLC8A1 and TXNDC17 in cancer performed by IHC, and *in vitro* and *in vivo* assays upon transient silencing of both proteins in CRC cells confirmed the association of both proteins to CRC survival and to CRC metastasis to the liver. Furthermore, both proteins were found to increase in the plasma of CRC patients at early stages (TXNDC17) and of individuals with premalignant lesions (SLC8A1 and TXNDC17) in comparison with healthy individuals, showing their quantification in plasma a high diagnostic ability of CRC at early stages of the disease.

## ASSOCIATED CONTENT

### Data Availability Statement

The mass spectrometry proteomics data have been deposited at the ProteomeXchange Consortium *via* the PRIDE partner repository with the data set identifier PXD039630.

### Supporting Information

The Supporting Information is available free of charge at <https://pubs.acs.org/doi/10.1021/acs.jproteome.3c00749>.

TMM SL normalization of MaxQuant data (Figure S1); differential expression analysis of TMT experiments (Figure S2); protein enrichment analysis of the dysregulated proteins in CRC progression (Figure S3); bioinformatics analysis and WB validation of proteins dysregulated in CRC (Figure S4); information of the paired tissue samples from CRC patients used for TMT and WB analysis (Table S1); information of plasma samples used by ELISA (Table S2); list of antibodies and reagents used for WB and IHC (Table S4); Uncropped WB and PCR images (File S1) ([PDF](#))

List of proteins identified and quantified by 10-Plex TMT quantitative proteomics experiments using paired FFPE samples from CRC patients (healthy, adenoma, and adenocarcinoma tissue samples) (Table S3) ([XLSX](#))

## AUTHOR INFORMATION

### Corresponding Authors

**Ana Montero-Calle** – Chronic Disease Programme (UFIEC), Instituto de Salud Carlos III, E-28220 Madrid, Spain; Proteomics Core UCCTs, Instituto de Salud Carlos III, E-28220 Madrid, Spain; Phone: +34-918223875; Email: [ana.monteroc@isciii.es](mailto:ana.monteroc@isciii.es)

**Rodrigo Barderas** – Chronic Disease Programme (UFIEC), Instituto de Salud Carlos III, E-28220 Madrid, Spain; Proteomics Core UCCTs, Instituto de Salud Carlos III, E-28220 Madrid, Spain; CIBER of Frailty and Healthy Aging (CIBERFES), E-28029 Madrid, Spain; [orcid.org/0000-0003-3539-7469](https://orcid.org/0000-0003-3539-7469); Phone: +34-918223231; Email: [r.barderasm@isciii.es](mailto:r.barderasm@isciii.es)

### Authors

**María Garranzo-Asensio** – Chronic Disease Programme (UFIEC), Instituto de Salud Carlos III, E-28220 Madrid, Spain

**Carmen Poves** – Gastroenterology Unit, Hospital Universitario Clínico San Carlos, E-28040 Madrid, Spain

**Rodrigo Sanz** – *Surgical Digestive Department, Hospital Universitario Clínico San Carlos, E-28040 Madrid, Spain*  
**Jana Dziakova** – *Surgical Digestive Department, Hospital Universitario Clínico San Carlos, E-28040 Madrid, Spain*  
**Alberto Peláez-García** – *Molecular Pathology and Therapeutic Targets Group, Hospital La Paz Institute for Health Research (IdiPAZ), E-28046 Madrid, Spain*  
**Vivian de los Ríos** – *Centro de Investigaciones Biológicas, CSIC, E-28040 Madrid, Spain*  
**Javier Martínez-Useros** – *Translational Oncology Division, OncoHealth Institute, Health Research Institute-Fundación Jiménez Díaz, Fundación Jiménez Díaz University Hospital/Universidad Autónoma de Madrid (IIS-FJD/UAM), E-28040 Madrid, Spain; Area of Physiology, Department of Basic Health Sciences, Faculty of Health Sciences, Rey Juan Carlos University, E-28922 Madrid, Spain*  
**María Jesús Fernández-Aceñero** – *Surgical Pathology Department, Hospital Clínico San Carlos, E-28040 Madrid, Spain*

Complete contact information is available at:  
<https://pubs.acs.org/10.1021/acs.jproteome.3c00749>

## Author Contributions

Conceptualization, A.M.-C. and R.B.; methodology, A.M.-C., M.G.-A., C.P., J.D., R.S., A.P.-G., V.R., J.M.-U., M.J.F.-A., and R.B.; investigation, A.M.-C., M.G.-A., C.P., J.D., R.S., A.P.-G., V.R., J.M.-U., M.J.F.-A., and R.B.; writing—original Draft, A.M.-C. and R.B.; writing—review and editing, A.M.-C., M.G.-A., A.P.-G., V.R., J.M.-U., M.J.F.-A., and R.B.; resources, A.P.-G., V.R., J.M.-U., M.J.F.-A., and R.B.; supervision, A.M.-C. and R.B.; and funding acquisition, R.B. All authors have read and approved the manuscript.

## Notes

The authors declare no competing financial interest.

**Ethical Approval And Consent To Participate** The study was conducted according to the guidelines of the Declaration of Helsinki, and approved by the Ethics Committee of Hospital Universitario Clínico San Carlos and Instituto de Salud Carlos III (CEI PI 13\_2020-v2).

## ACKNOWLEDGMENTS

This work was supported by the financial support from PI20CIII/00019 and PI23CIII/00027 grants from the AES-ISCIII program cofounded by FEDER funds to R.B. The financial support provided by the European Innovation Council (EIC) through the EIC Pathfinder Open 2023 project (Grant No. 101130574) to R.B. is also acknowledged. The FPU predoctoral contract to A.M.-C. was supported by the Spanish Ministerio de Educación, Cultura y Deporte.

## REFERENCES

- Simon, K.; Simon, K. Colorectal cancer development and advances in screening. *Clin. Interventions Aging* **2016**, *11*, 967–976.
- Stratton, M. R.; Campbell, P. J.; Futreal, P. A. The cancer genome. *Nature* **2009**, *458* (7239), 719–724.
- Siegel, R. L.; Miller, K. D.; Sauer, A. G.; Fedewa, S. A.; Butterly, L. F.; Anderson, J. C.; Cerck, A.; Smith, R. A.; Jemal, A. Colorectal cancer statistics, 2020. CA: *Cancer J. Clin.* **2020**, *70*, 145–164.
- Dekker, E.; Tanis, P. J.; Vleugels, J. L. A.; Kasi, P. M.; Wallace, M. B. Colorectal cancer. *Lancet* **2019**, *394* (10207), 1467–1480.
- Society, A. C. Survival Rates for Colorectal Cancer 2020. <https://www.cancer.org/cancer/colon-rectal-cancer>.
- Fearon, E. R. Molecular genetics of colorectal cancer. *Annu. Rev. Pathol.* **2011**, *6*, 479–507.
- Kuipers, E. J.; Grady, W. M.; Lieberman, D.; Seufferlein, T.; Sung, J. J.; Boelens, P. G.; van de Velde, C. J.; Watanabe, T. Colorectal cancer. *Nat. Rev. Dis. Primers* **2015**, *1*, No. 15065.
- Lambrechts, D.; Wauters, E.; Boeckx, B.; Aibar, S.; Nittner, D.; Burton, O.; Bassez, A.; Decaluwe, H.; Pircher, A.; Van den Eynde, K.; et al. Phenotype molding of stromal cells in the lung tumor microenvironment. *Nat. Med.* **2018**, *24* (8), 1277–1289.
- Koi, M.; Carethers, J. M. The colorectal cancer immune microenvironment and approach to immunotherapies. *Future Oncol.* **2017**, *13* (18), 1633–1647.
- Tauriello, D. V. F.; Batlle, E. Targeting the Microenvironment in Advanced Colorectal Cancer. *Trends Cancer* **2016**, *2* (9), 495–504.
- Garranzo-Asensio, M.; Segundo-Acosta, P. S.; Poves, C.; Fernandez-Acenero, M. J.; Martinez-Useros, J.; Montero-Calle, A.; Solis-Fernandez, G.; Sanchez-Martinez, M.; Rodriguez, N.; Ceron, M. A.; et al. Identification of tumor-associated antigens with diagnostic ability of colorectal cancer by in-depth immunomic and seroproteomic analysis. *J. Proteomics* **2020**, *214*, No. 103635.
- Barderas, R.; Mendes, M.; Torres, S.; Bartolome, R. A.; Lopez-Lucendo, M.; Villar-Vazquez, R.; Pelaez-Garcia, A.; Fuente, E.; Bonilla, F.; Casal, J. I. In-depth characterization of the secretome of colorectal cancer metastatic cells identifies key proteins in cell adhesion, migration, and invasion. *Mol. Cell. Proteomics* **2013**, *12* (6), 1602–1620.
- Mendes, M.; Pelaez-Garcia, A.; Lopez-Lucendo, M.; Bartolome, R. A.; Calvino, E.; Barderas, R.; Casal, J. I. Mapping the Spatial Proteome of Metastatic Cells in Colorectal Cancer. *Proteomics* **2017**, *17* (19), No. 1700094, DOI: [10.1002/pmic.201700094](https://doi.org/10.1002/pmic.201700094).
- Barderas, R.; Babel, I.; Casal, J. I. Colorectal cancer proteomics, molecular characterization and biomarker discovery. *Proteomics Clin. Appl.* **2010**, *4* (2), 159–178.
- Babel, I.; Barderas, R.; Diaz-Uriarte, R.; Martinez-Torrecuadrada, J. L.; Sanchez-Carbayo, M.; Casal, J. I. Identification of tumor-associated autoantigens for the diagnosis of colorectal cancer in serum using high density protein microarrays. *Mol. Cell. Proteomics* **2009**, *8* (10), 2382–2395.
- Coscia, F.; Lengyel, E.; Duraiswamy, J.; Ashcroft, B.; Bassani-Sternberg, M.; Wierer, M.; Johnson, A.; Wroblewski, K.; Montag, A.; Yamada, S. D.; et al. Multi-level Proteomics Identifies CT45 as a Chemosensitivity Mediator and Immunotherapy Target in Ovarian Cancer. *Cell* **2018**, *175* (1), 159–170.e116.
- Domon, B.; Aebersold, R. Mass spectrometry and protein analysis. *Science* **2006**, *312* (5771), 212–217.
- Aebersold, R.; Mann, M. Mass spectrometry-based proteomics. *Nature* **2003**, *422* (6928), 198–207.
- Martínez-Aguilar, J.; Chik, J.; Nicholson, J.; Semaan, C.; McKay, M. J.; Molloy, M. P. Quantitative mass spectrometry for colorectal cancer proteomics. *Proteomics Clin. Appl.* **2013**, *7* (1–2), 42–54.
- Buczak, K.; Ori, A.; Kirkpatrick, J. M.; Holzer, K.; Dauch, D.; Roessler, S.; Endris, V.; Lasitschka, F.; Parca, L.; Schmidt, A.; et al. Spatial Tissue Proteomics Quantifies Inter- and Intratumor Heterogeneity in Hepatocellular Carcinoma (HCC). *Mol. Cell. Proteomics* **2018**, *17* (4), 810–825.
- Dapic, I.; Baljeu-Neuman, L.; Uwuguiaren, N.; Kers, J.; Goodlett, D. R.; Corthals, G. L. Proteome analysis of tissues by mass spectrometry. *Mass Spectrom. Rev.* **2019**, *38* (4–5), 403–441.
- Coscia, F.; Doll, S.; Bech, J. M.; Schweizer, L.; Mund, A.; Lengyel, E.; Lindebjerg, J.; Madsen, G. I.; Moreira, J. M.; Mann, M. A streamlined mass spectrometry-based proteomics workflow for large-scale FFPE tissue analysis. *J. Pathol.* **2020**, *251* (1), 100–112.
- Guo, T.; Li, L.; Zhong, Q.; Rupp, N. J.; Charmpi, K.; Wong, C. E.; Wagner, U.; Rueschoff, J. H.; Jochum, W.; Fankhauser, C. D.; et al. Multi-region proteome analysis quantifies spatial heterogeneity of prostate tissue biomarkers. *Life Sci. Alliance* **2018**, *1* (2), No. 10.26508/lsa.201800042, DOI: [10.26508/lsa.201800042](https://doi.org/10.26508/lsa.201800042).

- (24) Peláez-García, A.; Barderas, R.; Torres, S.; Hernandez-Varas, P.; Teixido, J.; Bonilla, F.; de Herreros, A. G.; Casal, J. I. FGFR4 role in epithelial-mesenchymal transition and its therapeutic value in colorectal cancer. *PLoS One* **2013**, *8* (5), No. e63695.
- (25) Babel, I.; Barderas, R.; Díaz-Uriarte, R.; Martínez-Torrecuadrada, J. L.; Sánchez-Carbayo, M.; Casal, J. I. Identification of tumor-associated autoantigens for the diagnosis of colorectal cancer in serum using high density protein microarrays. *Mol. Cell. Proteomics* **2009**, *8* (10), 2382–2395.
- (26) Morikawa, K.; Walker, S. M.; Nakajima, M.; Pathak, S.; Jessup, J. M.; Fidler, I. J. Influence of organ environment on the growth, selection, and metastasis of human colon carcinoma cells in nude mice. *Cancer Res.* **1988**, *48* (23), 6863–6871.
- (27) Morikawa, K.; Walker, S. M.; Jessup, J. M.; Fidler, I. J. In vivo selection of highly metastatic cells from surgical specimens of different primary human colon carcinomas implanted into nude mice. *Cancer Res.* **1988**, *48* (7), 1943–1948.
- (28) Depciuch, J.; Klebowski, B.; Stec, M.; Szatanek, R.; Weglarczyk, K.; Baj-Krzyworzeka, M.; Parlinska-Wojtan, M.; Baran, J. Similarities in the General Chemical Composition of Colon Cancer Cells and Their Microvesicles Investigated by Spectroscopic Methods—Potential Clinical Relevance. *Int. J. Mol. Sci.* **2020**, *21* (5), No. 1826.
- (29) Montero-Calle, A.; Garranzo-Asensio, M.; Rejas-Gonzalez, R.; Feliu, J.; Mendiola, M.; Pelaez-Garcia, A.; Barderas, R. Benefits of FAIMS to Improve the Proteome Coverage of Deteriorated and/or Cross-Linked TMT 10-Plex FFPE Tissue and Plasma-Derived Exosomes Samples. *Proteomes* **2023**, *11* (4), No. 35, DOI: 10.3390/proteomes11040035.
- (30) Wiśniewski, J. R.; Gaugaz, F. Z. Fast and sensitive total protein and Peptide assays for proteomic analysis. *Anal. Chem.* **2015**, *87* (8), 4110–4116.
- (31) Solís-Fernández, G.; Montero-Calle, A.; Martínez-Useros, J.; Lopez-Janeiro, A.; de Los Rios, V.; Sanz, R.; Dziakova, J.; Milagrosa, E.; Fernandez-Acenero, M. J.; Pelaez-Garcia, A.; et al. Spatial Proteomic Analysis of Isogenic Metastatic Colorectal Cancer Cells Reveals Key Dysregulated Proteins Associated with Lymph Node, Liver, and Lung Metastasis. *Cells* **2022**, *11* (3), No. 447, DOI: 10.3390/cells11030447.
- (32) Solís-Fernández, G.; Montero-Calle, A.; Sanchez-Martinez, M.; Pelaez-Garcia, A.; Fernandez-Acenero, M. J.; Pallares, P.; Alonso-Navarro, M.; Mendiola, M.; Hendrix, J.; Hardisson, D.; et al. Aryl-hydrocarbon receptor-interacting protein regulates tumorigenic and metastatic properties of colorectal cancer cells driving liver metastasis. *Br. J. Cancer* **2022**, *126* (11), 1604–1615.
- (33) Montero-Calle, A.; Coronel, R.; Garranzo-Asensio, M.; Solis-Fernandez, G.; Rabano, A.; de Los Rios, V.; Fernandez-Acenero, M. J.; Mendes, M. L.; Martinez-Useros, J.; Megias, D.; et al. Proteomics analysis of prefrontal cortex of Alzheimer's disease patients revealed dysregulated proteins in the disease and novel proteins associated with amyloid-beta pathology. *Cell. Mol. Life Sci.* **2023**, *80* (6), No. 141.
- (34) Perez-Riverol, Y.; Bai, J.; Bandla, C.; Garcia-Seisdedos, D.; Hewapathirana, S.; Kamatchinathan, S.; Kundu, D. J.; Prakash, A.; Frericks-Zipper, A.; Eisenacher, M.; et al. The PRIDE database resources in 2022: a hub for mass spectrometry-based proteomics evidences. *Nucleic Acids Res.* **2022**, *50* (D1), D543–D552.
- (35) Szklarczyk, D.; Gable, A. L.; Lyon, D.; Junge, A.; Wyder, S.; Huerta-Cepas, J.; Simonovic, M.; Doncheva, N. T.; Morris, J. H.; Bork, P.; et al. STRING v11: protein-protein association networks with increased coverage, supporting functional discovery in genome-wide experimental datasets. *Nucleic Acids Res.* **2019**, *47* (D1), D607–D613.
- (36) Cerami, E.; Gao, J.; Dogrusoz, U.; Gross, B. E.; Sumer, S. O.; Aksoy, B. A.; Jacobsen, A.; Byrne, C. J.; Heuer, M. L.; Larsson, E.; et al. The cBio cancer genomics portal: an open platform for exploring multidimensional cancer genomics data. *Cancer Discovery* **2012**, *2* (5), 401–404.
- (37) Montero-Calle, A.; López-Janeiro, A.; Mendes, M. L.; Perez-Hernandez, D.; Echevarría, I.; Ruz-Caracuel, I.; Heredia-Soto, V.; Mendiola, M.; Hardisson, D.; Argüeso, P.; et al. In-depth quantitative proteomics analysis revealed C1GALT1 depletion in ECC-1 cells mimics an aggressive endometrial cancer phenotype observed in cancer patients with low C1GALT1 expression. *Cell. Oncol.* **2023**, *46*, 697–715.
- (38) Montero-Calle, A.; de Cedron, M. G.; Quijada-Freire, A.; Solis-Fernandez, G.; Lopez-Alonso, V.; Espinosa-Salinas, I.; Pelaez-Garcia, A.; Fernandez-Acenero, M. J.; Ramirez de Molina, A.; Barderas, R. Metabolic Reprogramming Helps to Define Different Metastatic Tropisms in Colorectal Cancer. *Front. Oncol.* **2022**, *12*, No. 903033.
- (39) Garranzo-Asensio, M.; Solis-Fernandez, G.; Montero-Calle, A.; Garcia-Martinez, J. M.; Fiua, M. C.; Pallares, P.; Palacios-Garcia, N.; Garcia-Jimenez, C.; Guzman-Aranguez, A.; Barderas, R. Seroreactivity Against Tyrosine Phosphatase PTPRN Links Type 2 Diabetes and Colorectal Cancer and Identifies a Potential Diagnostic and Therapeutic Target. *Diabetes* **2022**, *71* (3), 497–510.
- (40) Bardou, P.; Mariette, J.; Escudie, F.; Djemiel, C.; Klopp, C. jvnn: an interactive Venn diagram viewer. *BMC Bioinf.* **2014**, *15*, No. 293.
- (41) Wilmarth, P. Exploring Data Normalization and Analysis in Large TMT Experimental Designs. OHSU PSR Core 2018. [https://pwlmart.github.io/IRS\\_normalization/understanding\\_IRS.html](https://pwlmart.github.io/IRS_normalization/understanding_IRS.html).
- (42) Bartolome, R. A.; Barderas, R.; Torres, S.; Fernandez-Acenero, M. J.; Mendes, M.; Garcia-Foncillas, J.; Lopez-Lucendo, M.; Casal, J. I. Cadherin-17 interacts with alpha2beta1 integrin to regulate cell proliferation and adhesion in colorectal cancer cells causing liver metastasis. *Oncogene* **2014**, *33* (13), 1658–1669.
- (43) Li, M.; Jiang, X.; Wang, G.; Zhai, C.; Liu, Y.; Li, H.; Zhang, Y.; Yu, W.; Zhao, Z. ITGB4 is a novel prognostic factor in colon cancer. *J. Cancer* **2019**, *10* (21), 5223–5233.
- (44) Rey, C.; Soubeyran, I.; Mahouche, I.; Pedeboscq, S.; Bessede, A.; Ichas, F.; De Giorgi, F.; Lartigue, L. HIPK1 drives p53 activation to limit colorectal cancer cell growth. *Cell Cycle* **2013**, *12* (12), 1879–1891.
- (45) Deepa, S. S.; Dong, L. Q. APPL1: role in adiponectin signaling and beyond. *Am. J. Physiol.-Endocrinol. Metab.* **2009**, *296* (1), E22–E36.
- (46) Macklin, A.; Khan, S.; Kislinger, T. Recent advances in mass spectrometry based clinical proteomics: applications to cancer research. *Clin. Proteomics* **2020**, *17*, No. 17.
- (47) de Wit, M.; Fijneman, R. J.; Verheul, H. M.; Meijer, G. A.; Jimenez, C. R. Proteomics in colorectal cancer translational research: biomarker discovery for clinical applications. *Clin. Biochem.* **2013**, *46* (6), 466–479.
- (48) Álvarez-Chaver, P.; De Chiara, L.; Martínez-Zorzano, V. S. Proteomic Profiling for Colorectal Cancer Biomarker Discovery. In *Methods in Molecular Biology*; Springer, 2018; Vol. 1765, pp 241–269.
- (49) Butta cavoli, M.; Albanese, N. N.; Roz, E.; Pucci-Minafra, I.; Feo, S.; Cancemi, P. Proteomic Profiling of Colon Cancer Tissues: Discovery of New Candidate Biomarkers. *Int. J. Mol. Sci.* **2020**, *21* (9), No. 3096.
- (50) Ludvigsen, M.; Thorlacius-Ussing, L.; Vorum, H.; Stender, M. T.; Thorlacius-Ussing, O.; Honore, B. Proteomic Characterization of Colorectal Cancer Tissue from Patients Identifies Novel Putative Protein Biomarkers. *Curr. Issues Mol. Biol.* **2021**, *43* (2), 1043–1056.
- (51) Wiśniewski, J. R.; Dus-Szachniewicz, K.; Ostasiewicz, P.; Ziolkowski, P.; Rakus, D.; Mann, M. Absolute Proteome Analysis of Colorectal Mucosa, Adenoma, and Cancer Reveals Drastic Changes in Fatty Acid Metabolism and Plasma Membrane Transporters. *J. Proteome Res.* **2015**, *14* (9), 4005–4018.
- (52) Shao, Y.; Xu, K.; Zheng, X.; Zhou, B.; Zhang, X.; Wang, L.; Sun, Y.; Li, D.; Chen, T.; Wang, J.; et al. Proteomics profiling of colorectal cancer progression identifies PLOD2 as a potential therapeutic target. *Cancer Commun.* **2022**, *42* (2), 164–169.
- (53) Mu, Y.; Chen, Y.; Zhang, G.; Zhan, X.; Li, Y.; Liu, T.; Li, G.; Li, M.; Xiao, Z.; Gong, X.; Chen, Z. Identification of stromal differentially expressed proteins in the colon carcinoma by quantitative proteomics. *Electrophoresis* **2013**, *34* (11), 1679–1692.

- (54) Ku, X.; Xu, Y.; Cai, C.; Yang, Y.; Cui, L.; Yan, W. In-Depth Characterization of Mass Spectrometry-Based Proteomic Profiles Revealed Novel Signature Proteins Associated with Liver Metastatic Colorectal Cancers. *Anal. Cell. Pathol.* **2019**, *2019*, No. 7653230.
- (55) Xia, Y.; Yang, J.; Li, C.; Hao, X.; Fan, H.; Zhao, Y.; Tang, J.; Wan, X.; Lian, S.; Yang, J. TMT-Based Quantitative Proteomics Analysis Reveals the Panoramic Pharmacological Molecular Mechanism of beta-Elemonic Acid Inhibition of Colorectal Cancer. *Front. Pharmacol.* **2022**, *13*, No. 830328.
- (56) Zhu, H.; Li, Y.; Guo, J.; Feng, S.; Ge, H.; Gu, C.; Wang, M.; Nie, R.; Li, N.; Wang, Y.; et al. Integrated proteomic and Phosphoproteomic analysis for characterization of colorectal cancer. *J. Proteomics* **2023**, *274*, No. 104808.
- (57) Cianfrocco, M. A.; DeSantis, M. E.; Leschziner, A. E.; Reck-Peterson, S. L. Mechanism and regulation of cytoplasmic dynein. *Annu. Rev. Cell Dev. Biol.* **2015**, *31*, 83–108.
- (58) Schroer, T. A. Dynactin. *Annu. Rev. Cell Dev. Biol.* **2004**, *20*, 759–779.
- (59) Wang, S.; Wang, Q.; Zhang, X.; Liao, X.; Wang, G.; Yu, L.; Zhang, W.; Zhou, Q.; Hu, S.; Yuan, W. Distinct prognostic value of dynactin subunit 4 (DCTN4) and diagnostic value of DCTN1, DCTN2, and DCTN4 in colon adenocarcinoma. *Cancer Manage. Res.* **2018**, *10*, 5807–5824.
- (60) Wang, Q.; Wang, X.; Liang, Q.; Wang, S.; Liao, X.; Li, D.; Pan, F. Prognostic Value of Dynactin mRNA Expression in Cutaneous Melanoma. *Med. Sci. Monit.* **2018**, *24*, 3752–3763.
- (61) Busam, K. J.; Kutzner, H.; Cerroni, L.; Wiesner, T. Clinical and pathologic findings of Spitz nevi and atypical Spitz tumors with ALK fusions. *Am. J. Surg. Pathol.* **2014**, *38* (7), 925–933.
- (62) Bransfield, K. L.; Askham, J. M.; Leek, J. P.; Robinson, P. A.; Mighell, A. J. Phenotypic changes associated with DYNACTIN-2 (DCTN2) over expression characterise SJSA-1 osteosarcoma cells. *Mol. Carcinog.* **2006**, *45* (3), 157–163.
- (63) Su, X.; Li, H.; Chen, S.; Qin, C. Study on the Prognostic Values of Dynactin Genes in Low-Grade Glioma. *Technol. Cancer Res. Treat.* **2021**, *20*, No. 15330338211010143.
- (64) Paris, A.; Tardif, N.; Galibert, M. D.; Corre, S. AhR and Cancer: From Gene Profiling to Targeted Therapy. *Int. J. Mol. Sci.* **2021**, *22* (2), No. 752.
- (65) Oudekirk, J. L.; Krendel, M. Non-muscle myosins in tumor progression, cancer cell invasion, and metastasis. *Cytoskeleton* **2014**, *71* (8), 447–463.
- (66) Cao, R.; Chen, J.; Zhang, X.; Zhai, Y.; Qing, X.; Xing, W.; Zhang, L.; Malik, Y. S.; Yu, H.; Zhu, X. Elevated expression of myosin X in tumours contributes to breast cancer aggressiveness and metastasis. *Br. J. Cancer* **2014**, *111* (3), 539–550.
- (67) Schramek, D.; Sendoel, A.; Segal, J. P.; Beronja, S.; Heller, E.; Oristian, D.; Reva, B.; Fuchs, E. Direct *in vivo* RNAi screen unveils myosin IIa as a tumor suppressor of squamous cell carcinomas. *Science* **2014**, *343* (6168), 309–313.
- (68) Huang, Y. Q.; Han, Z. D.; Liang, Y. X.; Lin, Z. Y.; Ling, X. H.; Fu, X.; Cai, C.; Bi, X. C.; Dai, Q. S.; Chen, J. H.; et al. Decreased expression of myosin light chain MYL9 in stroma predicts malignant progression and poor biochemical recurrence-free survival in prostate cancer. *Med. Oncol.* **2014**, *31* (1), No. 820.
- (69) Matsushita, K.; Kobayashi, S.; Akita, H.; Konno, M.; Asai, A.; Noda, T.; Iwagami, Y.; Asaoka, T.; Gotoh, K.; Mori, M.; et al. Clinicopathological significance of MYL9 expression in pancreatic ductal adenocarcinoma. *Cancer Rep.* **2022**, *5* (10), No. e1582.
- (70) Lu, Y.; Liu, P.; Wen, W.; Grubbs, C. J.; Townsend, R. R.; Malone, J. P.; Lubet, R. A.; You, M. Cross-species comparison of orthologous gene expression in human bladder cancer and carcinogen-induced rodent models. *Am. J. Transl. Res.* **2010**, *3* (1), 8–27.
- (71) Feng, M.; Dong, N.; Zhou, X.; Ma, L.; Xiang, R. Myosin light chain 9 promotes the proliferation, invasion, migration and angiogenesis of colorectal cancer cells by binding to Yes-associated protein 1 and regulating Hippo signaling. *Bioengineered* **2022**, *13* (1), 96–106.
- (72) Zhao, B.; Baloch, Z.; Ma, Y.; Wan, Z.; Huo, Y.; Li, F.; Zhao, Y. Identification of Potential Key Genes and Pathways in Early-Onset Colorectal Cancer Through Bioinformatics Analysis. *Cancer Control* **2019**, *26* (1), No. 1073274819831260.
- (73) An, C. H.; Son, H. J.; Yoo, N. J.; Lee, S. H. Downregulation of a putative tumor suppressor gene PHRF1 in gastric and colorectal cancers. *Pathol. Res. Pract.* **2020**, *216* (6), No. 152984.
- (74) Prunier, C.; Zhang, M. Z.; Kumar, S.; Levy, L.; Ferrigno, O.; Tzivion, G.; Atfi, A. Disruption of the PHRF1 Tumor Suppressor Network by PML-RARalpha Drives Acute Promyelocytic Leukemia Pathogenesis. *Cell Rep.* **2015**, *10* (6), 883–890.
- (75) Ettahar, A.; Ferrigno, O.; Zhang, M. Z.; Ohnishi, M.; Ferrand, N.; Prunier, C.; Levy, L.; Bourgeade, M. F.; Bieche, I.; Romero, D. G.; et al. Identification of PHRF1 as a tumor suppressor that promotes the TGF-beta cytostatic program through selective release of TGIF-driven PML inactivation. *Cell Rep.* **2013**, *4* (3), 530–541.
- (76) Wang, Y.; Wang, H.; Pan, T.; Li, L.; Li, J.; Yang, H. Overexpression of PHRF1 attenuates the proliferation and tumorigenicity of non-small cell lung cancer cells. *Oncotarget* **2016**, *7* (39), 64360–64370.
- (77) Lee, J. Y.; Fan, C. C.; Chou, N. L.; Lin, H. W.; Chang, M. S. PHRF1 promotes migration and invasion by modulating ZEB1 expression. *PLoS One* **2020**, *15* (7), No. e0236876.
- (78) Oshima, K.; Amin, A. R. M. R.; Suzuki, A.; Hamaguchi, M.; Matsuda, S. SHPS-1, a multifunctional transmembrane glycoprotein. *FEBS Lett.* **2002**, *519* (1–3), 1–7.
- (79) Huijbers, E. J. M.; van der Werf, I. M.; Faber, L. D.; Sialino, L. D.; van der Laan, P.; Holland, H. A.; Cimpean, A. M.; Thijssen, V.; van Beijnum, J. R.; Griffioen, A. W. Targeting Tumor Vascular CD99 Inhibits Tumor Growth. *Front. Immunol.* **2019**, *10*, No. 651.
- (80) Mannion, A. J.; Odell, A. F.; Taylor, A.; Jones, P. F.; Cook, G. P. Tumour cell CD99 regulates transendothelial migration via CDC42 and actin remodelling. *J. Cell Sci.* **2021**, *134* (15), No. jsc240135, DOI: [10.1242/jcs.240135](https://doi.org/10.1242/jcs.240135).
- (81) Manara, M. C.; Bernard, G.; Lollini, P. L.; Nanni, P.; Zuntini, M.; Landuzzi, L.; Benini, S.; Lattanzi, G.; Sciandra, M.; Serra, M.; et al. CD99 acts as an oncosuppressor in osteosarcoma. *Mol. Biol. Cell* **2006**, *17* (4), 1910–1921.
- (82) Moutal, A.; Honnorat, J.; Massoma, P.; Desormeaux, P.; Bertrand, C.; Mallevalet, C.; Watrin, C.; Chounlamountri, N.; Mayeur, M. E.; Besancon, R.; et al. CRMP5 Controls Glioblastoma Cell Proliferation and Survival through Notch-Dependent Signaling. *Cancer Res.* **2015**, *75* (17), 3519–3528.
- (83) Ding, Y.; Cao, Y.; Wang, B.; Wang, L.; Zhang, Y.; Zhang, D.; Chen, X.; Li, M.; Wang, C. APPL1-Mediating Leptin Signaling Contributes to Proliferation and Migration of Cancer Cells. *PLoS One* **2016**, *11* (11), No. e0166172.
- (84) Liu, Y.; Zhang, C.; Zhao, L.; Du, N.; Hou, N.; Song, T.; Huang, C. APPL1 promotes the migration of gastric cancer cells by regulating Akt2 phosphorylation. *Int. J. Oncol.* **2017**, *51* (4), 1343–1351.
- (85) Pader, I.; Sengupta, R.; Cebula, M.; Xu, J.; Lundberg, J. O.; Holmgren, A.; Johansson, K.; Arner, E. S. Thioredoxin-related protein of 14 kDa is an efficient L-cystine reductase and S-dinitrosylase. *Proc. Natl. Acad. Sci. U.S.A.* **2014**, *111* (19), 6964–6969.
- (86) Espinosa, B.; Arner, E. S. J. Thioredoxin-related protein of 14 kDa as a modulator of redox signalling pathways. *Br. J. Pharmacol.* **2019**, *176* (4), 544–553.
- (87) Zhang, S. F.; Wang, X. Y.; Fu, Z. Q.; Peng, Q. H.; Zhang, J. Y.; Ye, F.; Fu, Y. F.; Zhou, C. Y.; Lu, W. G.; Cheng, X. D.; Xie, X. TXNDC17 promotes paclitaxel resistance via inducing autophagy in ovarian cancer. *Autophagy* **2015**, *11* (2), 225–238.
- (88) Peng, Q. H.; Yu, Y.; Cheng, X. D.; Wang, X. Y.; Lyu, W. G.; Xie, X.; Zhang, S. F. TXNDC17 protein overexpression in uterine papillary serous carcinoma is associated with clinicopathological characteristics and prognosis]. *Zhonghua Yi Xue Za Zhi* **2022**, *102* (32), 2506–2512.
- (89) Zhao, J.; Zhu, X.; Shrubsole, M. J.; Ness, R. M.; Hibler, E. A.; Cai, Q.; Long, J.; Chen, Z.; Jiang, M.; Kabagambe, E. K.; et al. Interactions between calcium intake and polymorphisms in genes

essential for calcium reabsorption and risk of colorectal neoplasia in a two-phase study. *Mol. Carcinog.* **2017**, *56* (10), 2258–2266.

(90) Xin, Y.; Shang, X.; Sun, X.; Xu, G.; Liu, Y.; Liu, Y. SLC8A1 antisense RNA 1 suppresses papillary thyroid cancer malignant progression via the FUS RNA binding protein (FUS)/NUMB like endocytic adaptor protein (Numbl) axis. *Bioengineered* **2022**, *13* (5), 12572–12582.

(91) Fadda, A.; Gentilini, D.; Moi, L.; Barault, L.; Leoni, V. P.; Sulas, P.; Zorcolo, L.; Restivo, A.; Cabras, F.; Fortunato, F.; et al. Colorectal cancer early methylation alterations affect the crosstalk between cell and surrounding environment, tracing a biomarker signature specific for this tumor. *Int. J. Cancer* **2018**, *143* (4), 907–920.

(92) Lai, X.; Lu, S.; Jiang, J.; Zhang, H.; Yang, Q.; Liu, Y.; Li, L.; Li, S.; Dai, S.; Chen, Y.; et al. Association of polymorphisms of calcium reabsorption genes SLC12A1, KCNJ1 and SLC8A1 with colorectal adenoma. *J. Cancer Res. Clin. Oncol.* **2023**, *149* (11), 8335–8344.

(93) Liu, Z.; Zhang, Y.; Niu, Y.; Li, K.; Liu, X.; Chen, H.; Gao, C. A systematic review and meta-analysis of diagnostic and prognostic serum biomarkers of colorectal cancer. *PLoS One* **2014**, *9* (8), No. e103910.

(94) Rodriguez-Cobos, J.; Vinal, D.; Poves, C.; Fernandez-Acenero, M. J.; Peinado, H.; Pastor-Morate, D.; Prieto, M. I.; Barderas, R.; Rodriguez-Salas, N.; Dominguez, G. DeltaNp73, TAp73 and Delta133p53 Extracellular Vesicle Cargo as Early Diagnosis Markers in Colorectal Cancer. *Cancers* **2021**, *13* (9), No. 2240.

(95) Brenne, S. S.; Madsen, P. H.; Pedersen, I. S.; Hveem, K.; Skorpen, F.; Krarup, H. B.; Giskeodegard, G. F.; Laugsand, E. A. Colorectal cancer detected by liquid biopsy 2 years prior to clinical diagnosis in the HUNT study. *Br. J. Cancer* **2023**, *129* (5), 861–868.

(96) Henderson, C. M.; Bollinger, J. G.; Becker, J. O.; Wallace, J. M.; Laha, T. J.; MacCoss, M. J.; Hoofnagle, A. N. Quantification by nano liquid chromatography parallel reaction monitoring mass spectrometry of human apolipoprotein A-I, apolipoprotein B, and hemoglobin A1c in dried blood spots. *Proteomics-Clin. Appl.* **2017**, *11* (7–8), No. 1600103, DOI: [10.1002/prca.201600103](https://doi.org/10.1002/prca.201600103).

(97) Kim, Y. J.; Gallien, S.; El-Khoury, V.; Goswami, P.; Sertamo, K.; Schlesser, M.; Berchem, G.; Domon, B. Quantification of SAA1 and SAA2 in lung cancer plasma using the isotype-specific PRM assays. *Proteomics* **2015**, *15* (18), 3116–3125.

(98) Campuzano, S.; Pedrero, M.; Barderas, R.; Pingarrón, J. M. Empowering Electrochemical Biosensing through Nanostructured or Multifunctional Nucleic Acid or Peptide Biomaterials. *Adv. Mater. Technol.* **2022**, *7*, No. 2200310.

(99) Garranzo-Asensio, M.; Guzman-Aranguez, A.; Povedano, E.; Ruiz-Valdepénas Montiel, V.; Poves, C.; Fernandez-Acenero, M. J.; Montero-Calle, A.; Solis-Fernandez, G.; Fernandez-Diez, S.; Camps, J.; et al. Multiplexed monitoring of a novel autoantibody diagnostic signature of colorectal cancer using HaloTag technology-based electrochemical immunosensing platform. *Theranostics* **2020**, *10* (7), 3022–3034.

(100) Montero-Calle, A.; Garranzo-Asensio, M.; Torrente-Rodriguez, R. M.; Montiel, V. R.-V.; Poves, C.; Dziakova, J.; Sanz, R.; del Arco, C. D.; Pingarron, J. M.; Fernandez-Acenero, M. J.; et al. p53 and p63 Proteoforms Derived from Alternative Splicing Possess Differential Seroreactivity in Colorectal Cancer with Distinct Diagnostic Ability from the Canonical Proteins. *Cancers* **2023**, *15* (7), No. 2102.